Distinct metabolic states of a cell guide alternate fates of mutational buffering through altered proteostasis

Kanika Verma[1,2,$], Kanika Saxena[1,$,#], Rajashekar Donaka[1], Aseem Chaphalkar[1], Manish Kumar Rai[1,2], Anurag Shukla[2,3], Zainab Zaidi[1], Rohan Dandage[1,2], Dhanasekaran Shanmugam[2,3], Kausik Chakraborty[1,2*]

[1] CSIR-Institute of Genomics and Integrative Biology, Mathura Road, Delhi, India 110025

[2] Academy of Scientific and Innovative Research, CSIR-HRDC, Ghaziabad, Uttar Pradesh, India-201002

[3] CSIR-National Chemical Laboratory, Pashan Road, Pune, India

[$] Equally contributing first authors

*Correspondence address kausik@igib.in, kausik@igib.res.in

[#]Institute of Biomedicine, University of Gothenburg, Medicinaregatan 7A, Gothenburg, Sweden

Summary

Changes in metabolism can alter the cellular milieu; can this also change intracellular proteostasis? Since proteostasis can modulate mutational buffering, if change in metabolism has the ability to change proteostasis, arguably, it should also alter mutational buffering. Building on this, we find that altered cellular metabolic states in *E. coli* buffer distinct mutations. Buffered-mutants had folding problems *in vivo* and were differently chaperoned in different metabolic states. Notably, this assistance was dependent upon the metabolites and not on the increase in canonical chaperone machineries. Additionally, we were able to reconstitute the folding assistance afforded by metabolites *in vitro* and propose that changes in metabolite concentrations have the potential to alter proteostasis. Collectively, we unravel that the metabolite pools are bona fide members of proteostasis and aid in mutational buffering. Given the plasticity in cellular metabolism, we posit that metabolic alterations may play an important role in positive or negative regulation of proteostasis.

Metabolic rewiring is a common response among different organisms to their surrounding environment[1]. Different cell types differ in their preferred mode of metabolism in order to harness energy and generate its required set of metabolites[2–5] It is also known to change with age and in case of metabolic diseases[6]. Since aging is associated with proteostasis defects, it is important to ask if change in metabolite composition of cellular milieu can alter intracellular protein folding capacity.

If metabolites and metabolism can affect proteostasis it may have two fundamental implications. 1) Metabolism-dependent change in proteostasis may aid evolution of the whole proteome when there is change in an organism's niche or surrounding climate, which alters its internal environment, or when an organism undergoes a large change in metabolism[5,7]. For example, some mutations may be rendered inactive in one metabolic state (a metabolic state is defined by the concentration of each of the metabolites the cell accumulates), while being active in a different one. Switching of metabolic niches may expose certain phenotypes that are hidden by metabolism-dependent genetic buffering. 2) tissue-specific metabolic differences may predispose cell-types to aggregate or misfold particular mutant protein, even while the protein is ubiquitously expressed. Age-dependent change in metabolism may also render certain tissues more prone to age-dependent aggregation[8,9]. This has important implications in explaining the late-onset tissue specificity of aggregation associated disorders[10] which has been hard to explain with our current understanding of proteostasis components.

Given the immediate importance of the second implication, the question should be asked with human diseases in mind[11]. However, given that metabolism is intricately linked to regulation of molecular chaperones through nutrient-signaling (TOR, gcn2, AMPK and so on) it is difficult to pin-point any proteostasis differences found in eukaryotic models to cellular milieu[12–15]. It will be hard to exclude the role of canonical molecular chaperones, autophagy or translation related mechanisms that are extensively studied[16–18]. Although these systems are extremely important in explaining cellular quality control, complexity of these machineries renders unmasking the role of cellular milieu in proteostasis a daunting task. In addition, the growth conditions for cell lines (specifically non-cancerous and untransformed cells needed in the study) are hardly defined. This places a limitation in understanding or altering metabolism in defined directions.

In order to address this fundamental question, we needed a bare minimum framework, an *in vivo* test tube, to test this possibility. We chose *E. coli* as it is well characterized in terms of its metabolic network, its chaperone content and the network of chaperones that work in the cytosol[19,20]. It also has few defined mechanisms to upregulate chaperones, which do not typically overlap with metabolism. We use this model and a newly devised assay to address the possibility of metabolism affecting mutational buffering.

While many studies have shown mixed results in terms of buffering by molecular chaperones- the proteins that aid in folding[21–25], remarkably little is known regarding role of cellular chemical milieu in proteostasis and mutational buffering. Previously we have shown that addition of small molecules at large concentrations in growth media leads to mutational buffering. Interestingly, the type of mutations buffered depended on the nature of the small molecule as different small molecules have different mechanisms to aid protein folding[26]. This indicated that molecular evolution can take different routes if different molecules are present in the growth media[27]. However, we do not understand if the physiological concentrations of metabolites present inside the cell affect protein folding and mutational buffering.

Osmolytes are abundant in cells and cells respond to osmotic shock by rewiring metabolism[7,28] which allows them to accumulate compensatory osmolytes[29]. Osmolytes also influence protein stability *in vitro* [27,30–33]. We hypothesized that change in osmotic composition of a cell may thus change protein folding, and hence mutational buffering. To test this, we used strains with altered level of certain osmolytes and monitored their potential to buffer mutations in two model proteins. Indeed the mutational buffering capacity was altered when the metabolite pools were altered. Interestingly, buffering capacity of the same strain in different metabolic states was different. In all cases mutational buffering was only evident for mutations that impair folding, corroborating the link between proteostasis and genetic buffering. Remarkably, the metabolites that change along with buffering capacity were able to aid protein folding *in vitro*, suggesting a strong link between metabolite-assisted protein folding and genetic buffering. Finally we proved the link between metabolic state and mutational buffering by evolving strains of *E. coli* with enhanced osmotic tolerance. These strains showed similar altered buffering capacity as seen for metabolically compromised cells, highlighting that protein folding environment is different in

different metabolic states. We propose that metabolic alterations can have far-reaching consequences on mutational buffering through their influence on proteostasis.

Results

Altered metabolite uptake leads to differences in mutational buffering

To elucidate if metabolic rewiring changes capacity to buffer mutations, we used two model proteins - Gentamicin-acetyl transferase (GmR, confers gentamicin resistance)[34] and Green Fluorescence Protein (GFP - yeast enhanced variant)[35]. These proteins met a few essential requirements. 1) Employing these model proteins we could monitor the activity of multiple mutants simultaneously. 2) These proteins are non-endogenous to *E. coli* and their activity is largely independent of endogeneous *E. coli* gene regulatory network except for the proteostasis network that takes care of its biogenesis and degradation. It ensured that altered buffering of different mutants of the proteins in different conditions is indeed an alteration in general mutational buffering capacity of *E. coli*. 3) The two proteins are unique protein-folds, presumably with different folding requirements. This enabled us to provide a fold-independent generality to the observations. 4) GFP was amenable to *in vitro* protein folding studies, helping us to reconstitute the buffering activities *in vitro*.

To generate a comprehensive map of mutational buffering, we developed massively-parallel activity assays to quantitate protein activity of a large number of mutants of the test proteins. Since Gm-R confers resistance to Gentamicin (Gm), we modified and developed a high throughput assay to quantitate protein activity using deep-mutational scanning[36]. We used a Glycine doublet mutant library for this protein[26](Figure **1A and S1A**). For the second test protein GFP, where we could isolate clones with different levels of GFP fluorescence, we used a random mutant library of GFP. Quantification of the intracellular folded fraction of GFP was done using flow-cytometry. Wt mCherry was expressed along with GFP as a bicistronic construct to control for differences in promoter activity and plasmid number (Figure **1B**).

To obtain *E. coli* strains with altered metabolism, we chose the strain CSH4[37] and a mutant strain on this background deleted of Proline and Glycine-betaine uptake transporters (WG350) (see Key resource table)[38].We chose this mutant as it is more osmosensitive than CSH4 (Figure **S1B**)

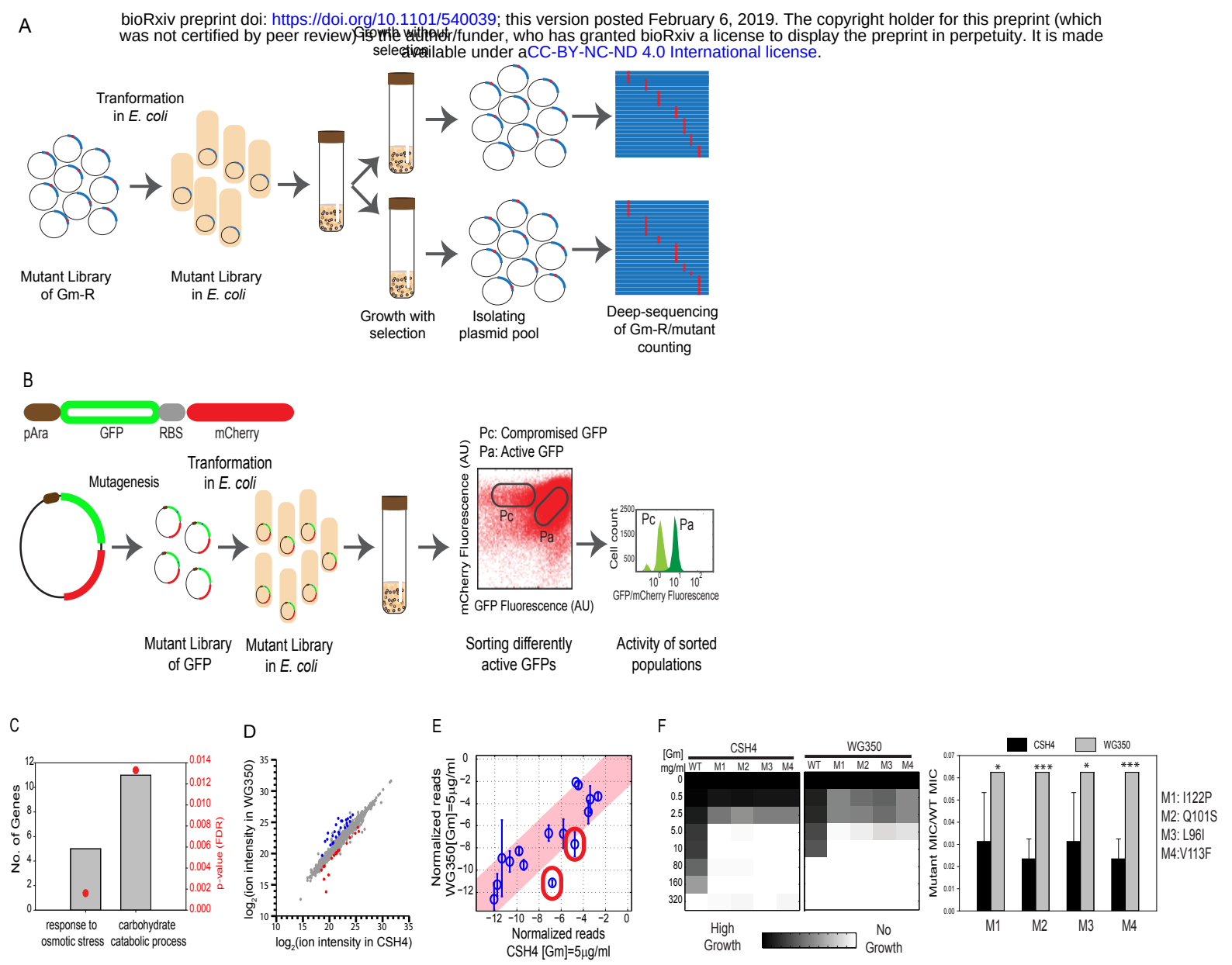

Figure 1: Genetic alteration in cellular metabolism changes mutational buffering

A. Schematic for highthroughput activity assay for Glycine-doublet substitution (GG-mutant) library of Gm-R. Activity of Gm-R mutants are inferred from the competitive fitness of the mutants in presence of Gm-selection. The competitive fitness for each of the mutants is quantified by deep-sequencing.

B. Schematic of highthroughput activity assay for GFP mutant library. The bi-cistronic construct of GFP and mCherry is driven by an arabinose inducible promoter. RBS indicates the position of the additional Ribosome Binding Site for translation of mCherry to serve as internal control. Mutations are created on GFP using random mutagenesis with GFP specific primers. Pool of GFP mutants are sorted into population of compromised mutants (Pc) and active mutants (Pa) based on GFP Fluorescence.

C. Gene Ontology (GO) classes that were upregulated in WG350 transcriptome with respect to CSH4. The fold enrichment is shown on the left-axis and Benjamini-Hochberg FDR corrected p-values for the enrichment score is shown on the right axis.

D. Comparison of metabolic features measured in WG350 and CSH4 using untargeted metabolomics. Metabolites features that are significantly different between CSH4 and WG350 are represented as colored circles (p-value < 0.05, 5 biological replicates for each sample).

E. Normalized read counts of Gm-R GG-mutant library at comparative selective pressures in the presence of the antibiotic gentamycin (Gm). Pink shaded area marks the 99% confidence interval. Mutants marked in red show lower read-counts in WG350 than in CSH4.

F. Left is a heat map representing growth of four Gm-R mutants in WG350 and in CSH4 along with Wt Gm-R in increasing concentration of Gm. Right panel shows the MIC of each of the mutants normalized with respect to Wt GmR in the respective strains. Error bars are representative of standard deviation from 4 biological replicates. Significance is calculated using student's t-test with respect to CSH4.

Also see Figure S1

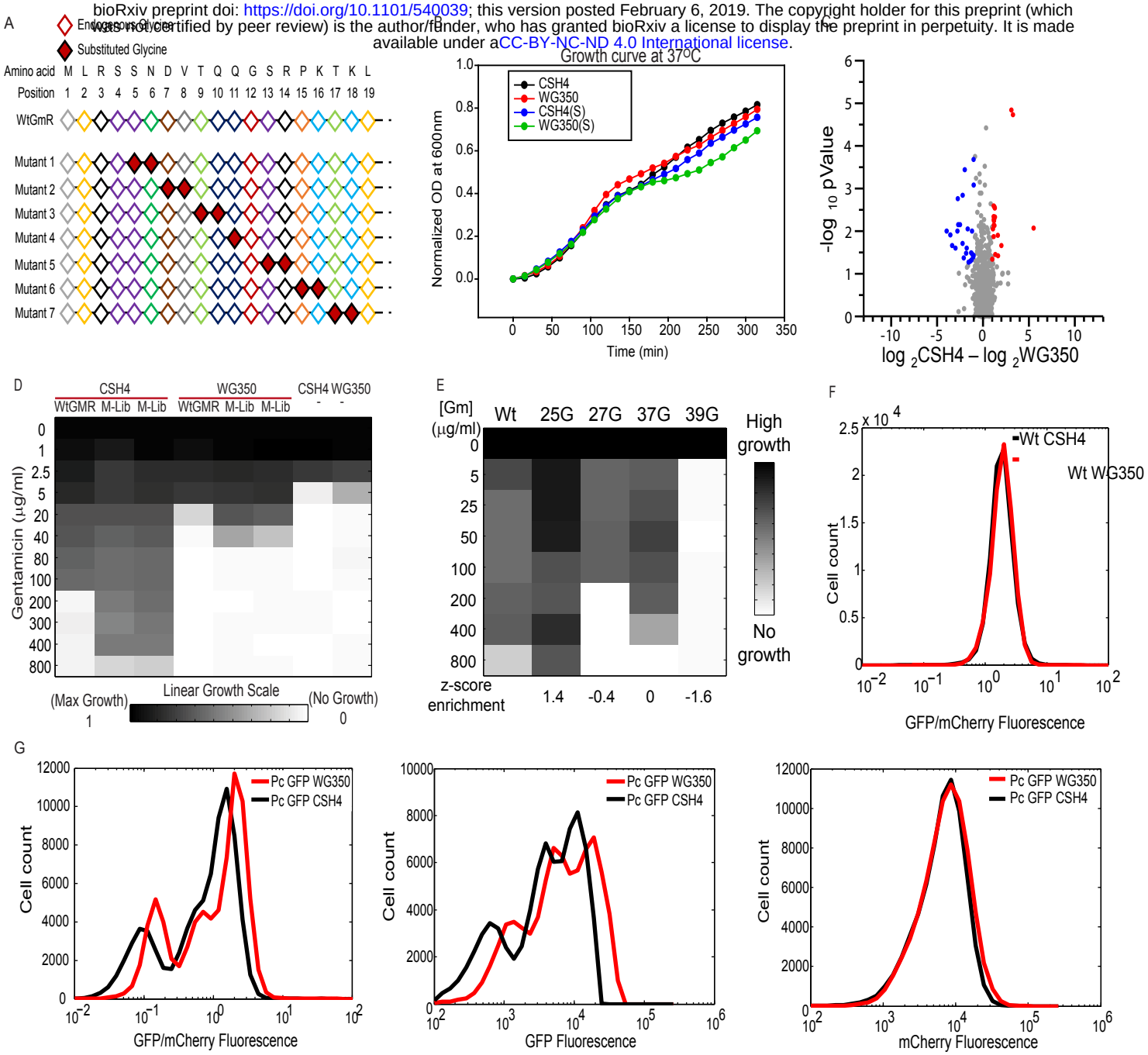

FIGURE S1: Strain specific metabolic differences lead to differential mutation buffering capacity (Related to Figure 1)

A. Schematic of Glycine doublet substitution library (GG) of Gm-R mutants where two consecutive amino acids have been substituted with two Glycine residues (red solid filled) starting from 5th amino acid.

B. Growth curve for E.coli strains CSH4 (black, blue) and WG350 (red, green) in presence and absence of 350 mM NaCl added in excess to the LB media while growing at 37°C.

C. Scatter plot for log2 of fold change in metabolite concentrations between CSH4 and WG350 against -log10 of p-value. The significantly altered metabolites (p-value < 0.05, 5 biological replicates for each sample) are shown in colored circles

D. Growth of untransformed CSH4 (-), WG350 (-) and cells transformed with Wt Gm-R and Glycine doublet mutant library plasmids (M-Lib) in increasing concentrations of Gentamicin (0-800mg/ml). Increase in growth is shown as increase in color density.

E. Correlation between NGS based quantification of enrichment scores (z-score) and MIC based semi-quantitative activity measurement for Wt Gm-R and mutants 25-26G, 27G, 37-38G, 39-40G of Glycine doublet mutant library.

F. Histogram for in vivo fluorescence of Wt GFP (represented as ratio of GFP/mCherry) in CSH4 (black) and WG350 (red)

G. Histogram for ratio of GFP/mCherry fluorescence and independent fluorescence of GFP and mCherry channel of mutant library Pc in CSH4 and WG350.

suggesting altered concentration of intracellular osmolytes; this served as an experimental model for alteration in its metabolism and osmolyte composition. To validate that deletion of uptake-transporters altered metabolism in the mutant strain we obtained the mRNAs differentially expressed between WG350 and CSH4 using RNA-seq; differentially expressed mRNAs were significantly enriched for genes encoding metabolic enzymes (Figure **1C**). To substantiate if the strains differed in terms of metabolite concentrations, we obtained untargeted metabolite profile for both the strains (Figure **1D, S1C**). The strains differed in terms of some of the metabolic features (43 metabolites with p-value <0.05). For example the metabolic features corresponding to Trehalose and Trehalose-6-Phosphate increased in WG350 compared to CSH4 by ~3 and ~4-fold, respectively (**Table S1**). Proline and Betaine, although the transporters were deleted in WG350, were only marginally lower (insignificant) in WG350 compared to CSH4 **(Table S1)**, indicating the cellular biosynthetic processes are switched on in the absence of transporters. This demonstrates that cellular metabolism is rewired significantly upon deletion of transporters of Proline and Glycine-betaine. Taken together metabolism in CSH4 and WG350 strains were significantly different; this provided us the platform to ask if mutational buffering differed between these strains that differed in metabolism.

To check for mutational buffering we transformed both the strains with Gm-R Glycine-duplet substitution (GmR-GG) library and grew them at similar selection pressure (see star methods for details) in the presence of Gentamicin (Gm) (Figure **S1D**). To check for mutation-specific effects it was important to normalize Minimal Inhibitory Concentrations (MICs) of the mutants with respect to that of Wt Gm-R as Wt Gm-R transformed WG350 was more sensitive to Gm than CSH4 with Wt Gm-R (Figure **S1D**). Mutant pools were sequenced and analyzed to obtain abundance of the different mutants in the presence or absence of selection pressure (Gentamicin in growth medium). Enrichment scores in the presence of Gm selection were calculated to quantitate their activity as previously published[36]. Enrichment scores (a measure of activity) of a chosen set of partially active and inactive mutants as identified with this assay, correlate well with the semi-quantitative measurements of activity as obtained by minimum-inhibitory concentration (MIC) of Gm in presence of each of these mutants (**Figure S1E**). Two of the Gm-R mutants (Gm-R (25G,26G) and Gm-R (27G)) were less active in WG350 than in CSH4, indicating mutation-specific differences buffering (**Figure 1E**). We confirmed that transcription/translation were not different in these strains using a GFP/mCherry system that is

driven by the same promoter (**Figure S1F**). Remarkably, another set of small molecule dependent Gm-R mutants used in a previous study[26] revealed higher activity wrt Wt Gm-R in WG350 than in CSH4 **(Figure 1F)**. This underlined that WG350 does not have a lower capacity to fold mutant proteins, but has a different spectrum of buffered mutants compared to CSH4.

For the second test protein with a completely different fold, we purified a population of GFP mutants (compromised fluorescence, Pc) that show lower GFP fluorescence compared with Wt GFP in the WT E. coli strain BW25113 (referred to as BW henceforth). Mutant pool Pc had similar fluorescence in CSH4 and WG350 strains (**Figure S1G**), demonstrating that the difference between the strains in buffering mutations is protein-specific. Taken together, this suggests that the ability to take up metabolites from the medium affects metabolic network and mutational buffering. This change the spectrum of mutations buffered in a protein-specific manner.

Different metabolic states of the same cell show differences in buffering capacity

Next we asked if altering metabolite pool in the same strain backgrounds change mutational buffering. Since osmotic shock alters the metabolite pool facilitating the accumulation of osmotically active metabolites[28], we grew the strains WG350 and CSH4 in 350mM NaCl to change the metabolic status of the cell. We obtained transcriptomic (**Figure 2A**) and metabolomic shifts (**Figure 2B, S2A**) associated with osmotic shock in each of the strain. Osmotic shock altered metabolism in both the strains (**Figure 2C, S2B**) but were routed differently in the two strains. For example, Fructose 1,6-bisphosphate was strongly upregulated in CSH4 upon osmotic shock but not in WG350, contrastingly, Succinate was upregulated in WG350 but not in CSH4 upon osmotic stress **(Table S1)**. Interestingly, the osmotic adaptation of CSH4 and WG350 strains led to a marked similarity in terms of their potential to buffer di-glycine mutations in Gm-R (**Figure 2D**). Gm-R(25G,26G) and Gm-R(27G,28G), mutants less active in WG350 than in CSH4, show similar activity in these strains in the presence of NaCl in the growth medium. The GG-mutants of Gm-R that showed enhanced activity in WG350 compared to CSH4, shows a noticeably smaller difference or similar activity in both the strains during osmotic shock (**Figure 2E**). This rules out the canonical effect of osmotic stress induced aggregation in affecting buffering under the conditions used here. Notably, buffering capacity of WG350 and CSH4 towards Gm-R was similar although the osmotic composition of the strains in

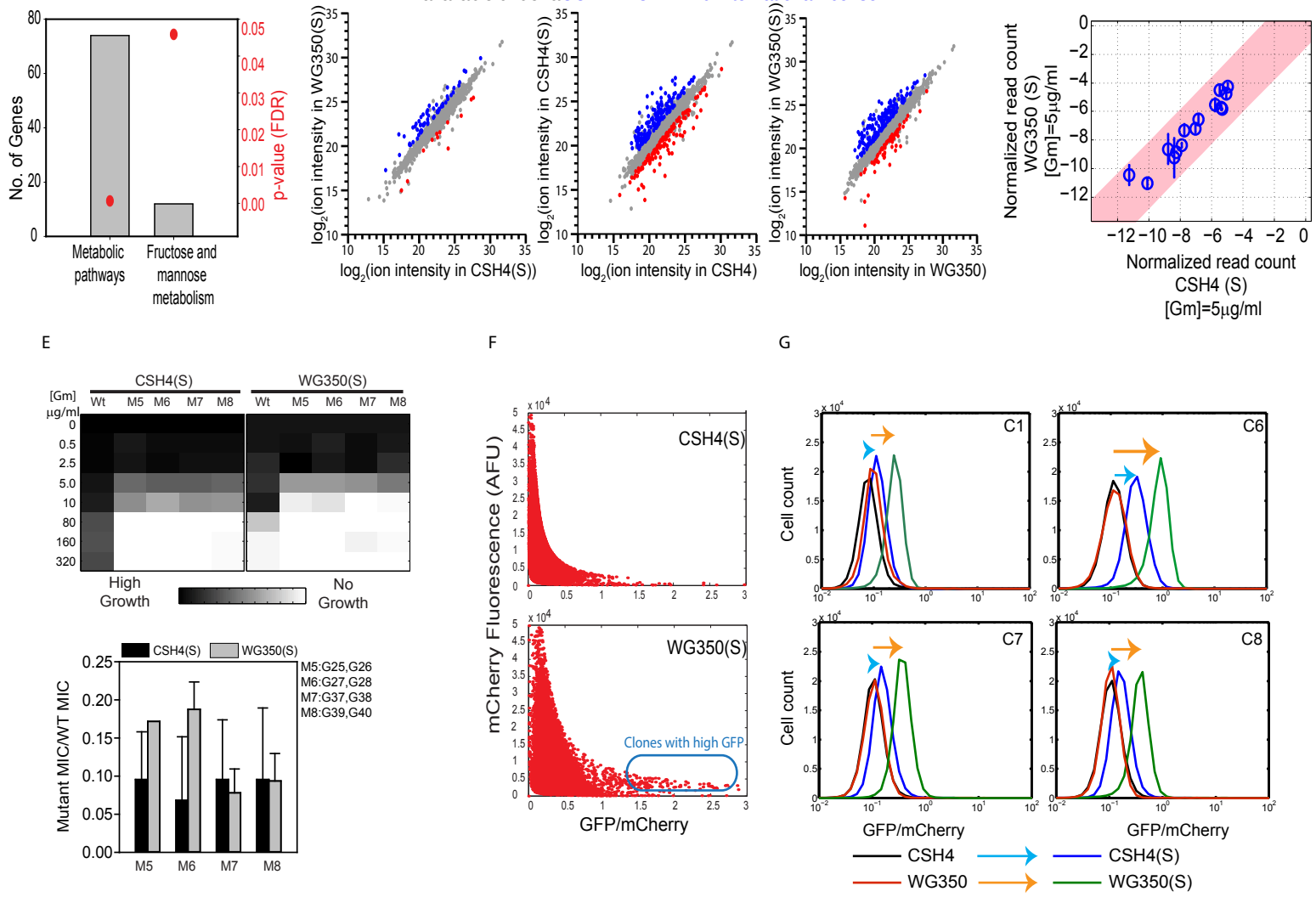

Figure 2: Osmotic stress-induced changes in metabolism changes the spectrum of mutants buffered

A. Gene Ontology (GO) classes that were upregulated in WG350 transcriptome with respect to CSH4 during osmotic shock. The fold enrichment is shown on the left-axis and Benjamini-Hochberg FDR corrected p-values for the enrichment score is shown on the right axis.

B. Comparison of metabolic features measured in WG350 and CSH4 during growth in media containing 350mM NaCl using untargeted metabolomics. The significantly different metabolites (p-value < 0.05, 5 biological replicates for each sample) are represented in colored circles.

C. Comparison of metabolic features within strain in presence and absence of 350mM NaCl in growth media. The significantly different metabolites (p-value < 0.05, 5 biological replicates for each sample) are represented in colored circles.

D. Normalized read counts of Gm-R GG-mutant library at comparative selective pressures in the presence of the antibiotic Gentamicin (Gm) and 350mM NaCl in the growth media. Pink shaded area marks the 99% confidence interval.

E. Left panel shows heat map representing activity (in terms of growth) of mutants described earlier (see Figure 1E) in CSH4 and WG350 grown in presence of 350mM NaCl and different concentration of Gm. Right panel shows the MIC of each of the mutants normalized with respect to Wt-GmR in the respective strains. Error bars are representative of standard deviation from 4 biological replicates.

F. Single cell fluorescence for the partially active pool of GFP mutants (Pc). The scatter plot for mCherry Vs GFP/mCherry fluorescence is shown for Pc in WG350 and CSH4 when grown in the presence of 350mM NaCl added in excess to the LB growth medium. Clones with high GFP fluorescence during osmotic stress in WG350 are indicated by the blue box.

G. Histogram of GFP/mCherry fluorescence of the Isolated clones (C1,C6, C7, and C8) in WG350 and CSH4 in the presence and absence of 350mM NaCl. The shift in the ratio due to osmotic shock is shown with colored arrows. The cyan arrow indicates increase/decrease in GFP fluorescence upon addition of 350mM NaCl to CSH4 strain, the orange arrow indicates the same for WG350.

Also see Figure S2

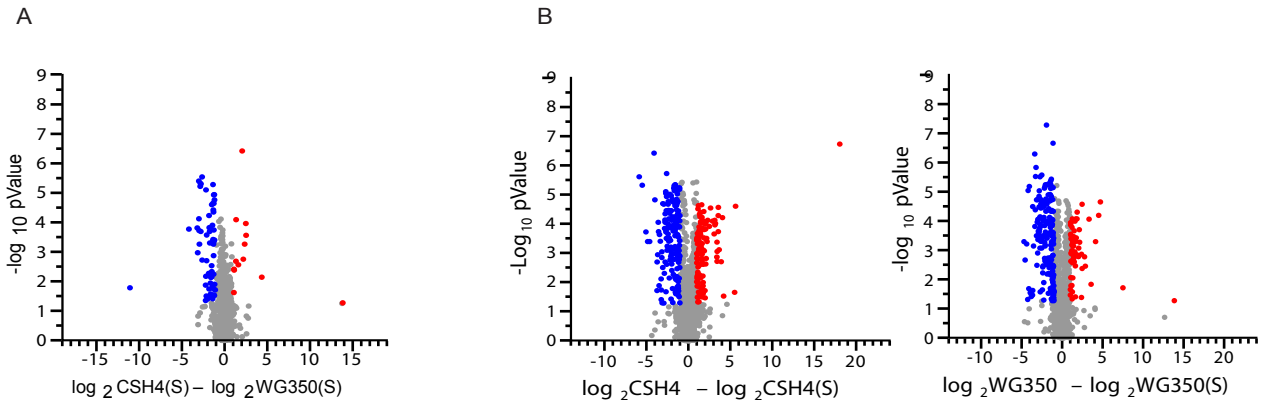

C

```
wt      MSKGEELFTGVVPILVELDGDVNGHKFSVSGEGEGDATYGKLTLKFICTTGKLPVPWPTL   60
c1      MSKGEELFTGVVPILVELDGDVNCHKFSVSGEGEGDATYGKLTLKFICTTGKLPVPWPTL   60
c6      MSKGEELFTGVVPILVELDGDVNGHKFSVSGEGEGDATYGKLTLKFICTTGKLPVPWPTL   60
c7      MSKGEELFTGVVPILVELDGDVNCHKFSVSGEGEGDATYGKLTLKFICTTGKLPVPWPTL   60
c8      MSKGEELFTGVVPILVELDGDVNCHKFSVSGEGEGDATYGKLTLKFICTTGKLPVPWPTL   60
        ************************ ************************************

wt      VTTFGYGVQCFARYPDHMKQHDFFKSAMPEGYVQERTIFFKDDGNYKTRAEVKFEGDTLV   120
c1      VTTFGYGVQCFARYPDHMKQHDFFKSAMPEGYVQERTIFFKDDGNYKTRAEVKFEGDTLV   120
c6      VTTFGYGVQCFARYPDHMKQHDFFKSAMPEGYVQERTIFFKNDGNYKTRAEVKFEGDTLV   120
c7      VTTFGYGVQCFARYPDHMKQHDFFKSAMPEGYVQERTIFFKDDGNYKTRAEVKFEGDTLV   120
c8      VTTFGYGVQCFARYPDHMKQHDFFKSAMPEGYVQERTIFFKDDGNYKTRAEVKFEGDTLV   120
        ************************************************:***************

wt      NRIELKGIDFKEDGNILGHKLEYNYNSHNVYIMADKQKNGIKVNFKIRHNIEDGSVQLAD   180
c1      NRIELKGIDFKEDGNILGHKLEYNYNSHNVYIMADKQKNGIKVNFKIRHNIEDGSVQLAD   180
c6      NRIELKGIDFKEDGNILGHKLEYNYNSHNVYIMADKQKNGIKVNFKIRHNIEDGSVQLAD   180
c7      NRIELKGIDFKEDGNILGHKLEYNYNSHNVYIMADKQKNGIKVNFKIRHNIEDGSVQLAD   180
c8      NRIELKGIDFKEDGNILGHKLEYNYNSHNVYIMADKQKNGIKVNFKIRHNIEDGSVQLAD   180
        ************************************************************

wt      HYQQNTPIGDGPVLLPDNHYLSTQSALSKDPNEKRDHMVLLEFVTAAGITHGMDELYK     238
c1      HYQQNTPIGDGPVLLPDNHYLSTQSALSKDPNEKRDHMVLLEFVTAAGITHGMDELYK     238
c6      HYQQNTPNGDGPVLLPDNHYLSTQSALSKDPNEKRDHMVLLEFVTAAGITHGMDELYK     238
c7      HYQQNTPIGDGPVLLPDNHYLSTQSALSKDPNEKRDHMVLLKFVTAAGITHGMDELYK     238
c8      HYQQNTPIGDGPVLLPDNHYLSTQSALSKDPNEKRDHMSLLEFVTAAGITHGMDELYK     238
        *******************************  **:*****************
```

FIGURE S2: Osmotic stress induced modification in cellular metabolism changes the subset of mutations buffered (Related to Figure 2)
A. Scatter plot for log2 of fold change in metabolic features between WG350 and CSH4 during osmotic shock against p-value. The significantly different metabolites (p-value < 0.05, 5 biological replicates for each sample) are represented in colored circles.
B. Scatter plot for log2 of fold change in metabolic features within strains CSH4 (left) and WG350 (right) on osmotic shock(s) against p-value. The significantly different metabolites (p-value < 0.05, 5 biological replicates for each sample) are represented in colored circles.
C. Amino acid sequence alignment of Wt GFP (YeGFP) with the isolated mutants C1, C6, C7, C8. Mutations are shown in red boxes.

the presence of the salt is different. This indicates that compensatory mechanisms may work through different metabolic pathways to reinstate similar spectrum of mutational buffering.

Since metabolite composition of WG350 and CSH4 were different in the presence of salt, and it is known that different small molecules have protein- and mutation-specific effects [27], we asked if there could be difference in mutational buffering for a different protein. Indeed mutational buffering of these strains during osmotic shock is different for the GFP mutant library (although for Gm-R it was the same) (**Figure 2F**). We could identify multiple clones of GFP that showed enhanced fluorescence in WG350 compared to CSH4 in the presence of osmotic shock. This clearly shows that the activity of these GFP mutants are enhanced in this altered osmotic condition. In order to validate the observed buffering, we isolated single clones from the pool using FACS and sequenced them. The clones segregated into two clusters; the first cluster contained a common mutation G24C while the second cluster with only one clone was devoid of this mutation (**Figure S2C**). Upon retransformation, each of these mutants exhibited similar fluorescence in CSH4 and WG350 in normal growth media while their fluorescence increased in osmotic stress (**Figure 2G**). Notably, these exhibited not only higher fluorescence in WG350 than in CSH4 in the presence of osmotic shock but different mutants were buffered to different extent in WG350 under osmotic stress. Hence, these clones confirm that difference in mutational buffering capacity of a strain is protein specific. Taken together, the evidences suggest that the alterations in cellular metabolism changes buffering capacity.

Mutational buffering is affected through altered proteostasis

Having obtained different clones of GFP we asked if mutational buffering has contribution from altered proteostasis. The mutations did not map close to the fluorophore of GFP suggesting that the fluorescence *per se* was not altered (**Figure S3A**). *In vitro* fluorescence of the purified mutants was similar to that of Wt GFP (**Figure 3A**) confirming that the mutations did not affect fluorescence of the folded proteins. Refolding studies of the purified proteins showed that the proteins have severely reduced refolding rate compared to the Wt protein (**Figure 3B**). Except for C6, the apparent rates for refolding were ~2 to ~10 fold lower than the refolding rates of Wt GFP (**Figure 3B**). This demonstrated that the mutants isolated were indeed folding-compromised mutants, thus differences in their *in vivo* fluorescence in different strains and conditions may reflect the differences in proteostasis capacities between strains.

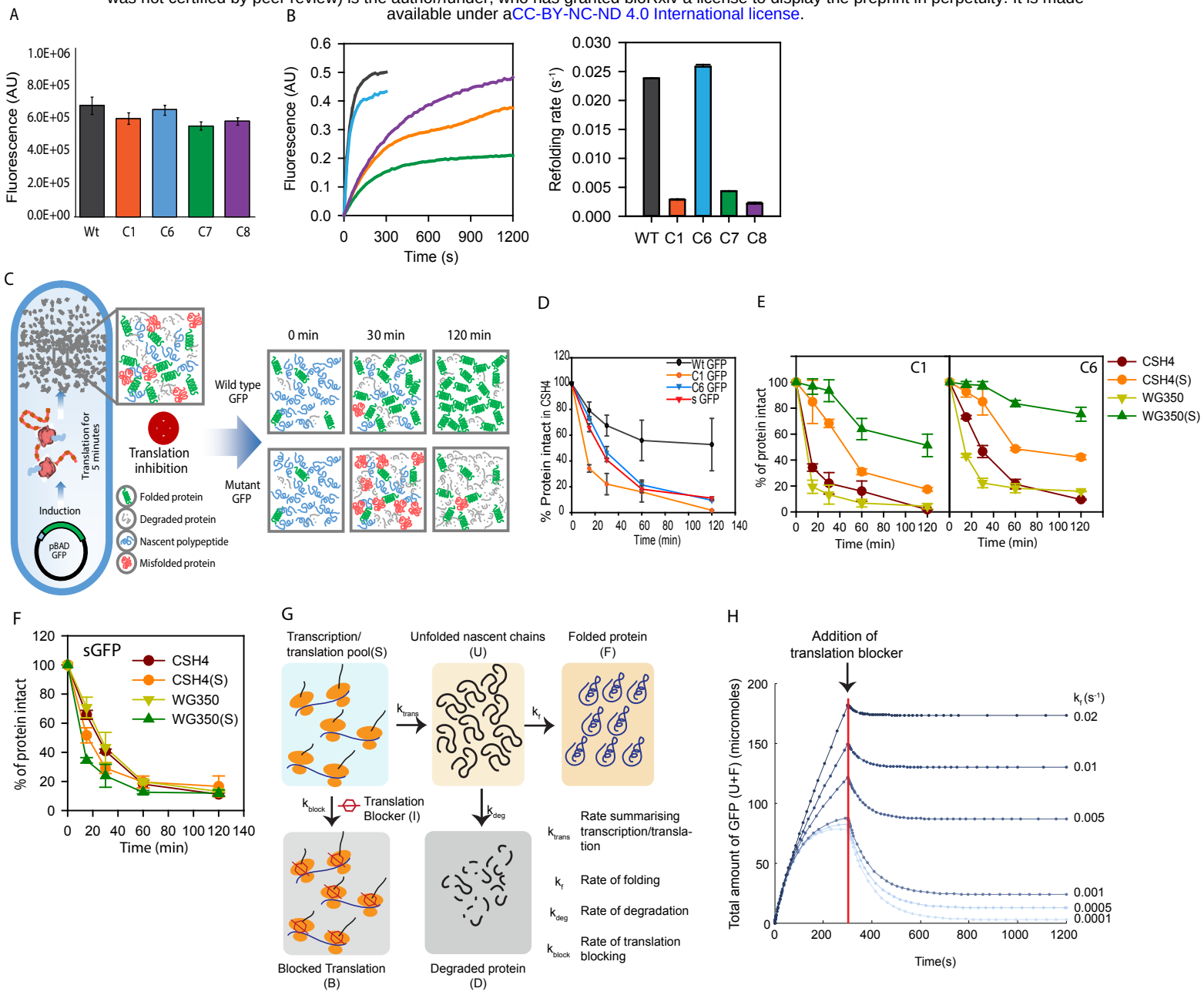

Figure 3: Mutations buffered by altered metabolic states have compromised protein folding

A. Fluorescence of each of the mutants and Wt-GFP at 515nm are shown at 200nM concentration (excitation 488nm /slit-width 2nm, emission slit-width 5nm).

B. Refolding of GFP and the mutants were initiated by unfolding the proteins in 6M GuHCl, followed by a 100-fold dilution into Buffer-A (50mM Tris, 150mM NaCl, 2mM DTT, pH 7.4) to a final concentration of 200nm for the proteins. Refolding was followed by monitoring GFP fluorescence as a function of time.

C. Schematic of Chloramphenicol-based chase for degradation of GFP as described in star methods. Briefly, after a short (5min) induction of GFP with 0.5% arabinose, translation was stalled with Chloramphenicol. Cells were lysed at different points and the amount of intact GFP was monitored by immunoblotting with anti-GFP antibody.

D. Plot for the gel-based quantification of intact GFP in Chloramphenicol-chase assay for monitoring degradation of GFP mutants and Wt GFP in CSH4.

E. Plot for the gel-based quantification of intact GFP in Chloramphenicol-chase assay for monitoring degradation of mutant GFPs in WG350(S)(WG350 grown in presence of 350mM NaCl), WG350, CSH4(S) (CSH4 grown in presence of 350mM NaCl) and CSH4.

F. Plot for the gel-based quantification of intact GFP in Chloramphenicol-chase assay for monitoring degradation of sGFP in CSH4, WG350, CSH4(S) and WG350(S).

G. Schematic for simulation setting. Numerical simulation was set up with a fixed concentration of mRNA/ribosome complex (S). These complexes could either form nascent polypeptides (U) with a rate ktrans that is a collective rate constant for transcription/translation, or be inhibited with a rate constant kblock in the presence of a translation inhibitor (I). The pool of U could either degrade with a rate kdeg or fold with a rate constant of kf and reach the native state (F). We finally monitor the total amount of undegraded protein (U+F) after blocking translation after 300(s) of starting the simulation (simulation start mimics induction).

H. Total amount of intact GFP obtained from simulation as a function of kf while keeping kdeg constant at 0.01 s-1. Red line indicates the time-point at a 1mM dose of translation-inhibitor (I) is added.

Also see Figure S3

A

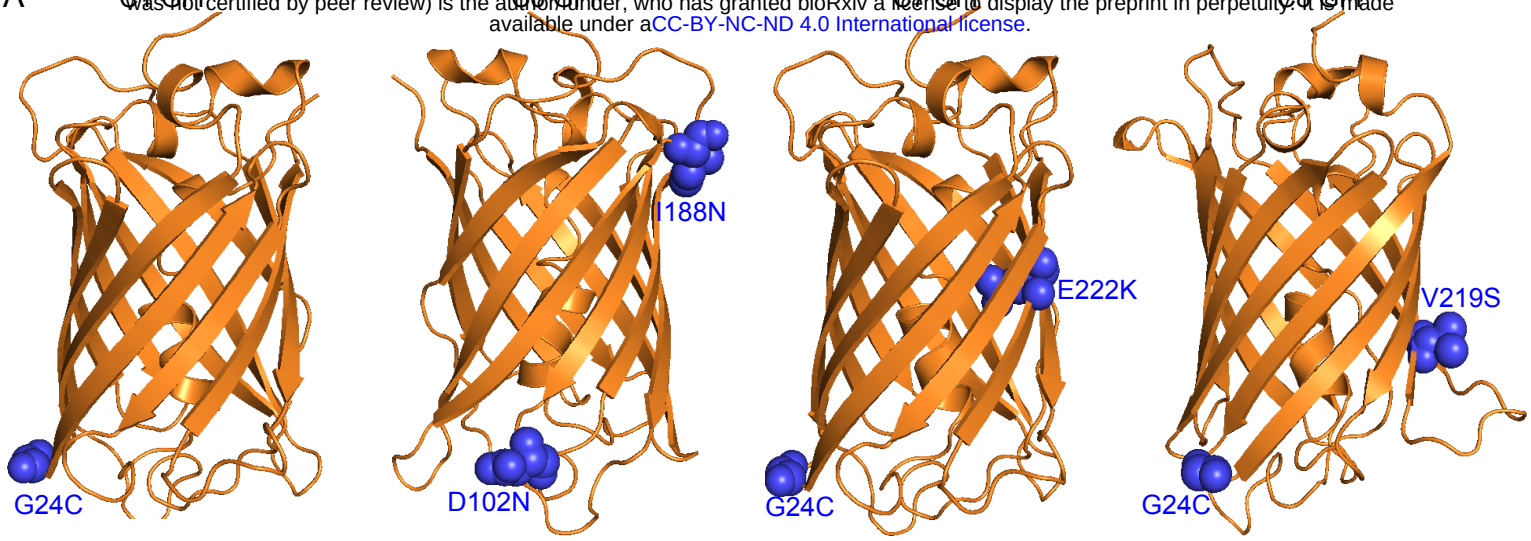

B

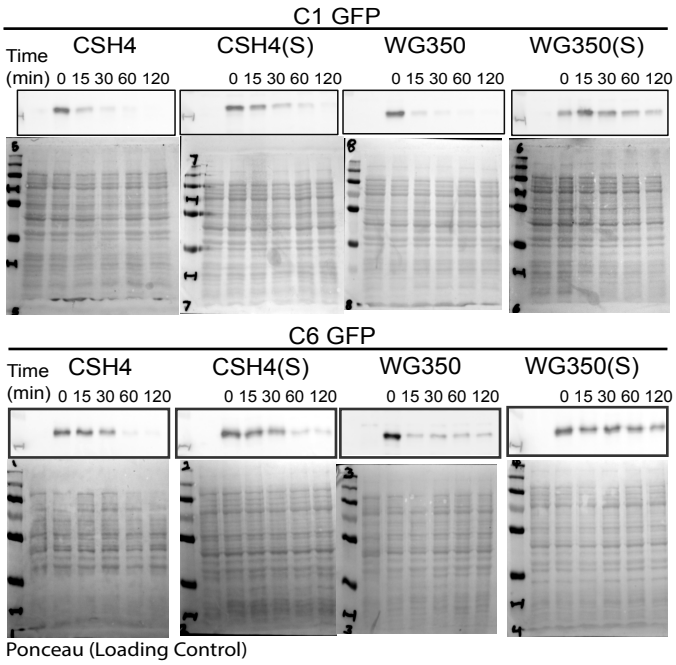

C

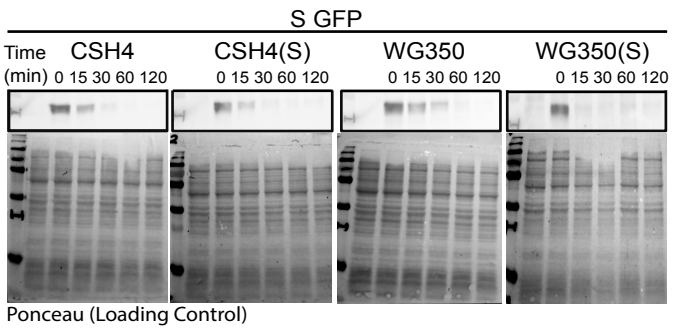

D

ODEs:
d(U)/dt = -ReactionFlux1 - ReactionFlux2 + ReactionFlux3
d(F)/dt = ReactionFlux1
d(S)/dt = -ReactionFlux3 - ReactionFlux4
d(B)/dt = ReactionFlux4
d(I)/dt = -ReactionFlux4

Fluxes:
ReactionFlux1 = kf*U
ReactionFlux2 = kd*U
ReactionFlux3 = ktrans*S
ReactionFlux4 = ki*S*I

Parameter Values:
$k_f = 0.02\ (s^{-1})$
$k_{deg} = 0.01\ (s^{-1})$
$k_{trans} = 0.001(s^{-1})$
$ki = 0.0001\ (M^{-1}s^{-1})$
cell volume = 1 (liters)

Initial Conditions (micromoles):
U = 0
F = 0
S= 1000
B = 0
I = 0

Dosing:
Delay : 300s
1mM of I added to reaction

FIGURE S3: Fluorescence increase is not due better proteostasis in WG350(S) (Related to Figure 3)

A. Mutations buffered in WG350 while growing in 350mM NaCl (C1, C6, C7, C8) are marked on the GFP crystal structure (pdb: 1GFL)(Yang, Moss and Phillips, 1996).

B. Representative images for immunoblotting to chase degradation of C1 and C6 GFP as described in star methods in CSH4 and WG350 in presence and absence of osmotic stress. GFP degrades slowest in WG350 (S). Ponceau has been used as loading control

C. Representative images for immunoblotting to chase degradation of sGFP in CSH4 and WG350 in presence and absence of osmotic stress. Ponceau has been used as loading control

D. ODEs used for the kinetic simulations. Numerical simulation was set up with a fixed concentration of mRNA/ribosome complex (S). These complexes could either form nascent polypeptides (U) with a rate ktrans that is a collective rate constant for transcription/translation, or be inhibited with a rate constant kblock in the presence of a translation inhibitor (I). The pool of U could either degrade with a rate kdeg or fold with a rate constant of kf and reach the native state (F). We finally monitor the total amount of undegraded protein (U+F) after blocking translation after 300(s) of starting the simulation (simulation start mimics induction). The reaction volume was kept at 1liter.

To check for *in vivo* folding defects for the isolated clones, we checked for the degradation rates of a representative set of mutants (slow folding and buffered- C1; fast folding and buffered- C6; fast-degrading and not buffered- sGFP vis a vis Wt GFP by stalling translation after briefly inducing protein expression in CSH4 **(Figure 3C)**. All the mutants degraded faster than Wt GFP underlining that these mutants are folding-compromised under *in vivo* conditions (**Figure 3D**).

To check if difference in proteostasis between WG350 and CSH4 with and without osmotic shock contributed towards differential buffering in the stains, we checked the degradation rates for the GFP mutants. The degradation rates of the mutant GFPs in CSH4 and WG350 were similar, however there was a sharp decrease in degradation rates of the C1 and C6 in WG350(S) (WG350 when grown in 350mM NaCl) compared to CSH4(S) (CSH4 when grown in 350mM NaCl)(**Figure 3E (graph), S3B(gel)**). This was not a general decrease in degradation capacity of the cell, as sGFP - a degradation prone mutants of GFP - degraded with similar kinetics in both the stains in the presence and absence of salt-stress (**Figure 3F (graph), S3C(gel)**). Furthermore, the general proteases were upregulated in WG350(S) rather than being downregulated (shown later in **Figure 4A)** arguing against a possible decrease in degradation capacity of WG350(S).

A simple kinetic simulation of protein synthesis followed by folding or quality control assisted degradation (**Figure 3G, S3D**) indicated that an increase in folding rate would be expected to show a decrease in degradation (**Figure 3H**). Thus the apparent decrease degradation rate may arise solely due to differences in folding rate in vivo in the different strains and conditions while the degradation rate remains constant (as seen for sGFP). Taken together this indicates that the mutants isolated were indeed folding mutants and mutational buffering differed between the strains due to their differences in proteostasis capacities.

The mutants are dependent on chemical chaperones and not on molecular chaperones

To investigate the contribution of molecular chaperones, we checked if their levels changed in WG350(S). Set of genes involved in maintaining protein quality control were expected to be induced (or repressed) in WG350(S) than in WG350, CSH4(S) or CSH4. However, mRNA levels of none of the chaperones or proteases other than DnaJ and HslU/V followed the expected over-expression pattern (**Figure 4A**). Protein levels of the canonical chaperones, GroEL and DnaK also did not differ significantly (**Figure 4B**).

Since we isolated specific clones, it provided us with the handle to ask if these mutants were dependent on the canonical abundant chaperones of the cytosol. Single deletions of the abundant canonical molecular chaperones (tig, dnaK, dnaJ, secB, ClpB)[20], or the proteases (lon, hslU/V, ClpX/P/A)[39,40], did not decrease fluorescence of these clones significantly (**Figure 4C**) suggesting that intracelluar folding of these mutants were independent of these proteostasis machineries. It would also mean that overexpression of DnaJ or HslU/V seen in WG350(S) at mRNA levels may not contribute to mutational buffering of the mutants. Coherently, overexpressing DnaK/DnaJ/GrpE or the GroEL/GroES system in CSH4 or WG350 did not increase the fluorescence of these mutants (**Figure 4D, S4A, S4B**), suggesting that the buffering effect in WG350(S) is independent of the concentration of these molecular chaperones. To mimic a global increase chaperone levels we used other environment stressors like heat shock and oxidative stress that are known to increase stress-response driven chaperone levels[20,41,42]. The fluorescence of the isolated clones that show enhanced folding in the presence of NaCl induced osmotic stress did not fluoresce better with heat or oxidative stress (**Figure 4E**).

In vitro, GroEL/ES machinery could only marginally accelerate the rate of refolding of GFP mutants C1 and C8, whereas in the presence of DnaK/J/GrpE, mutant C8 showed no difference in the refolding rate and mutant C1 showed a slight reduction in the rate of refolding (**Figure 4F**). This confirms that these mutants are not the substrates of the abundant chaperone machineries *in vivo* and *in vitro*. To investigate if molecular chaperones could assist the folding of these mutant GFPs in WG350(S) more efficiently, we studied the physical interaction of these polypeptides chains with molecular chaperones in WG350(S). To check this we performed *in vivo* crosslinking and measured the amount of higher-order complexes (possibly with components of proteostasis machinery) formed by the mutants GFPs in CSH4 and WG350 with and without osmotic shock (**Figure 4G, S4C**). The levels were not higher in WG350(S), indicating that chaperone association is not altered in WG350(S). Thus, strain-specific proteostasis differences that alter mutational buffering have contributions from components other than molecular chaperones.

Mutant-specificity and protein-specificity of folding assistance *in vivo* has been shown to be a hall-mark of chemical chaperone mediated folding. To confirm if these mutants were indeed dependent upon chemical chaperones for folding, we obtained their refolding rates in the

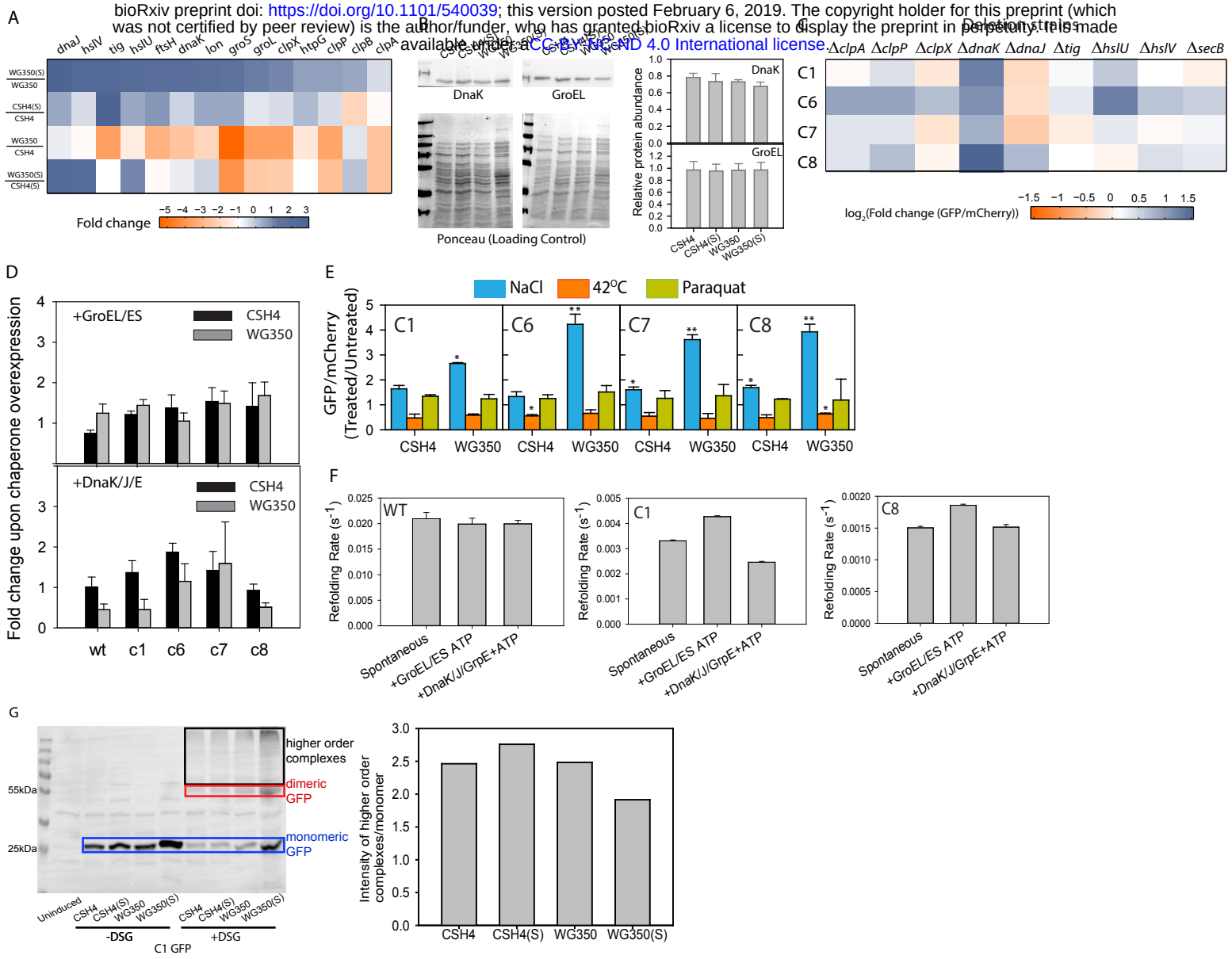

Figure 4: Folding of isolated mutants is independent of molecular chaperones

A. Heatmap representing relative quantification of transcripts encoding proteostasis related proteins in WG350 and CSH4 in the presence and absence of 350mM NaCl.

B. Right panel shows the immunoblot and left panel the image based quantitation of GroEL and DnaK expression levels in WG350 and CSH4 in the presence and absence of 350mM NaCl (p-value>0.05). Ponceu stained blot, used as loading control, is shown at the bottom of right panel.

C. Wt GFP and the mutants were expressed in WT E. coli (BW25113, BW) and in strains harboring single deletion of different molecular chaperones and proteases. GFP/mCherry for each of the mutants were normalized with respect to Wt GFP fluorescence in the same strains. Fold change in GFP/mCherry for each of the mutant GFPs between BW and the deletions strains was calculated using these normalized values. log2 values of this fold change is shown as heatmap.

D. Wt GFP and the mutants were expressed in WG350 or CSH4 with or without plasmids overexpressing either DnaK/J/E or GroEL/ES. Median GFP/mCherry fluorescence levels of Wt GFP and the mutants in the different strains are shown are a bargraph. Error bars represent standard deviation of 3 biological replicates (p-value>0.05).

E. Wt GFP and representative mutants were expressed in CSH4 and WH350 in the absence or presence of external stressors (42^{0}C - heat shock, 80µM Paraquat- oxidative stress, 350mM NaCl - osmotic shock). GFP/mCherry fluorescence of Wt GFP and mutants and shown in each of these conditions as bargraph with standard deviations as error bars from 3 biological replicates. Signifance is calculated using student's t test.

F. *In vitro* refolding Wt GFP and mutants were initiated as described earlier. To check chaperone dependence, unfolded proteins were diluted 100-fold in the presence of DnaK/DnaJ/GrpE (400nM/800nM/400nM, respectively) or GroEL/ES (400nM/800nM, respectively), and folding was initiated by adding 2mM ATP. Refolding was followed by monitoring GFP fluorescence as a function of time. Rate of refolding is plotted for Wt GFP and mutants of GFP in presence and absence of chaperoning machinery.

G. Immunoblotting for GFP showing the recruitment of nascently formed Wt GFP and mutant GFP into multiprotein complexes. After a brief induction of GFP (and mutant) expression, cells were treated with a cell-permeable crosslinker (DSG). Subsequent to crosslinking, cells were lysed and resolved on SDS-PAGE followed by immunoblotting with anti-GFP antibody. Free GFP (or mutants) are show with the blue box, dimeric GFP (or mutants) are shown in red box and multimeric complexes are shown in black box. The ratio of GFP in multimeric complex and the amount in monomeric state is shown in the accompanying bar graph.

Also see Figure S4

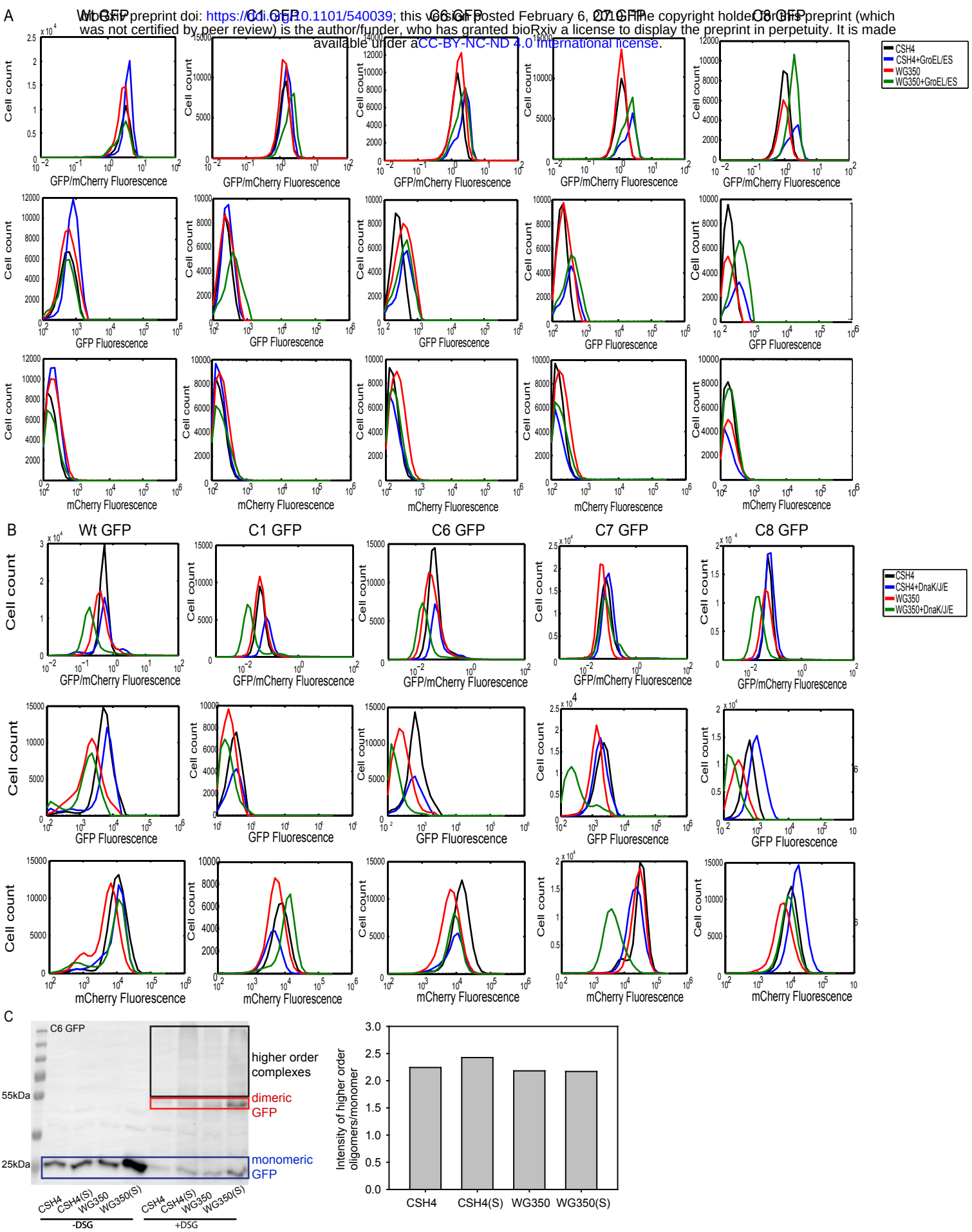

FIGURE S4: Observed buffering of GFP mutants is not channeled only through molecular chaperones (Related to Figure 4)

A. Histogram for GFP/mCherry Fluorescence (top panel), GFP (middle panel) and mCherry fluorescence (bottom panel) in absence of overexpressed GroEL/ES (black, red, 2 biological replicates) and while co-expressed with GroEL/ES (blue, green, 2 biological replicates) in CSH4 and WG350. Induction protocol was followed as described in Star Methods.

B. Histogram for GFP/mCherry Fluorescence (top panel), GFP (middle panel) and mCherry fluorescence (bottom panel) in absence of overexpressed DnaK/J/GrpE (black, red, 2 biological replicates) and while co-expressed with DnaK/J/GrpE (blue, green, 2 biological replicates) in CSH4 and WG350.

C. Immunoblotting for GFP showing the recruitment of nascently formed C6 GFP into multiprotein complexes. Free GFP (or mutants) are show with the blue box, dimeric GFP (or mutants) are shown in red box and the multimeric complexes are shown in black box. The ratio of GFP in multimeric complex and the amount in monomeric state is shown in the accompanying bar graph.

presence of different metabolites (**Figure 5A**). Many of the metabolites could act as chemical chaperones to accelerate the refolding rates. Molecules likes Aspartate, Glycine, chaperoned refolding of two of the mutants (albeit with mutation specific effect); C6 mutant did not show enhanced refolding rate with any of the small molecules tested. This reiterated the mutant specific effect of different chemical chaperones[26,27] and suggested that these small molecules could indeed facilitate the folding of these proteins and lead to mutational buffering. Of note, the space sampled in terms of cellular small-molecules was non-exhaustive and no combinations were tried.

To check if small molecule milieu of cells can aid folding we re-constituted *in vitro* refolding of the selected GFP mutants in small-molecule enriched cellular extract of WG350. Refolding of GuHCl unfolded GFP mutants were initiated by diluting out the denaturant in the presence of extract obtained from WG350 (**Figure 5B**). Interestingly, these mutants were refolded to only a negligible extent in the absence of extract while folding substantially in its presence, underlining the importance of the small molecule milieu of the cell in chaperoning protein folding. We confirmed that these lysates were free from proteins and hence molecular chaperones that are known to assist refolding. It is important to stress that the current technologies of extraction limits the concentration at which these small molecules can be extracted; they are more than a thousand fold diluted from their physiological concentrations. It is therefore difficult to recapitulate the full potential of this mixture, and reproduce the *in vivo* differences between strains. However, it demonstrates that the metabolite pool, even on dilution, acts as chaperone and hence can participate in cellular proteostasis. Hence, metabolic differences have the capacity to show altered mutational buffering in different metabolic states. This is primarily evident for mutations that destabilize proteins and make them sensitive to osmolyte concentrations.

Taken together, metabolic differences manifest differences in mutational buffering which may have a significant contribution from metabolite-dependent proteostasis.

Altering cellular metabolism using metabolites changes mutational buffering

Having realized that genetic and osmotic alteration of metabolism changes the spectrum of mutation buffering, we asked if other routes of altering metabolism may show similar changes in buffering. Addition of excess metabolites - like amino acids- is known to rewire metabolism[43].

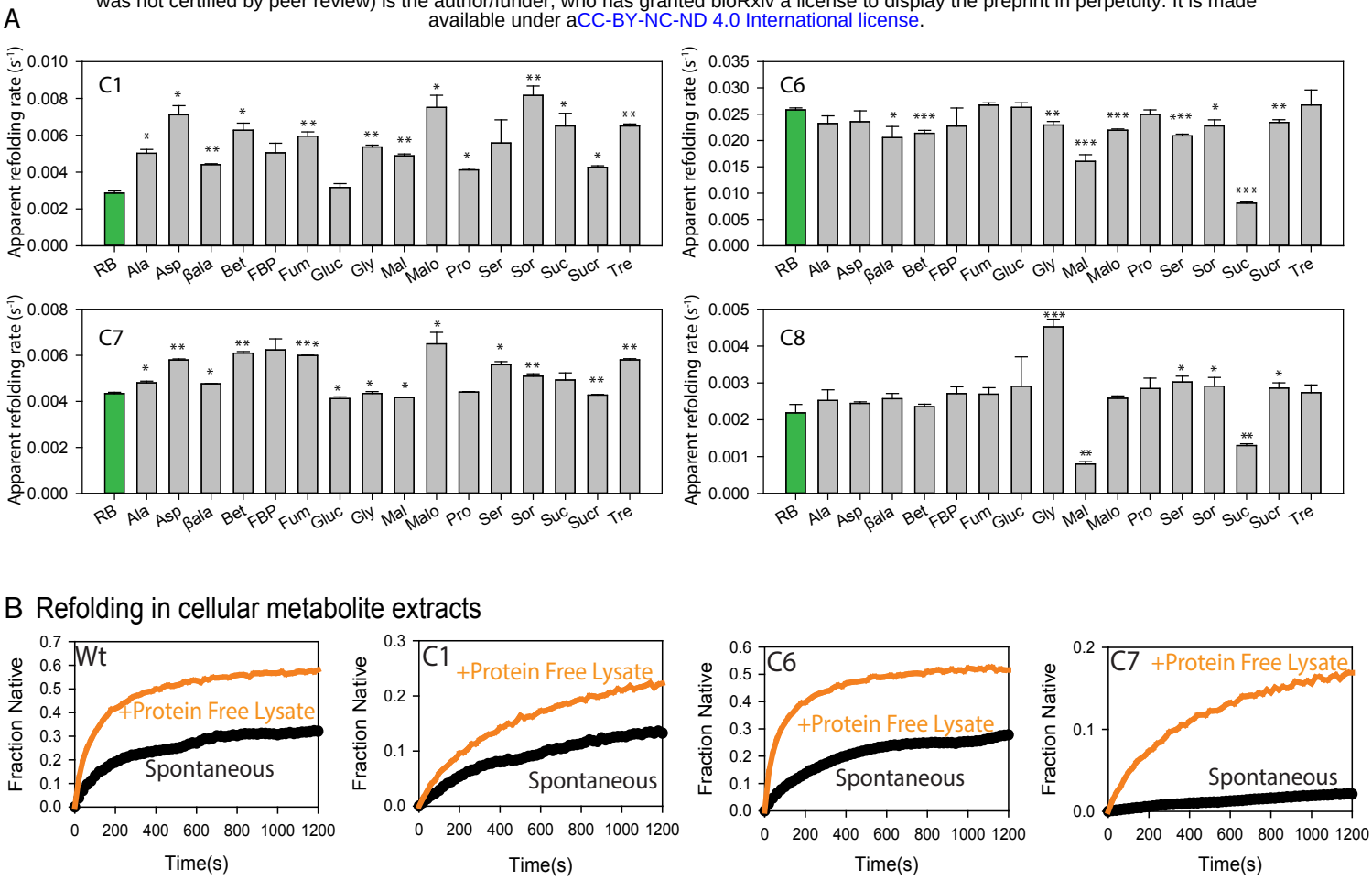

Figure 5: Metabolites can chaperone the mutants in vivo and in vitro.

A. Refolding of Wt GFP or mutant GFP was initiated as described earlier in the presence of 100mM concentration of different metabolites. Refolding rates were obtained by fitting the refolding traces with single exponential equations. Mean of refolding rates, along with standard deviations are shown for three replicates of refolding reactions. RB (shown in green bars) are refolding rates in Buffer-A, the base buffer in which the metabolites are added. P-value is calculated using students's t test with repect to RB. Ala:Alanine, Asp:Aspartate, βala: β alanine, Bet: Betaine, FBP: Fructose 1,6-bis-phosphate, Fum: Fumarate, Gluc: Glucose, Gly: Glycine, Mal: Malate, Malo:Malonate, Pro: Proline, Ser: Serine, Sor: Sorbitol, Suc: Succinate, Sucr: Sucrose, Tre: Trehalose.

B. Protein free extracts were isolated from WT E. coli (BW25113, BW) as described in Methods. Refolding was performed by diluting unfolded proteins (Wt GFP or mutants) 100-fold into these extracts.

We added excess of the amino acids, or sugars and other metabolites to rich media to alter metabolism and check for altered buffering. Exogenous addition of many of these compounds to growth media (individual concentrations provided in **Table S2**) also led to enhanced folding of some of mutants GFP in CSH4 *in vivo* (**Figure 6A**). Specifically, addition of Alanine increased the fluorescence of all the mutant proteins as seen *in vitro* (**Figure 6B**). Further demonstrating that the mutants isolated from the screen predominantly respond to proteostasis alterations due to differences in metabolites, and mutational buffering can be altered by altering cellular concentration of metabolites. Interestingly, different additives had mutant-specific chaperoning activity *in vivo* as seen *in vitro*. This unravels the complex connection between mutational buffering and metabolic status.

Metabolism is dependent on genetic background[43–45]. BW strain, a WT K-12 strain with a different genetic background, shows completely different pattern of mutational buffering for the mutant GFPs in the presence of the different metabolites (**Figure 6C**). The inactive pool of mutants also showed buffering in general in the presence of different metabolites. Remarkably, the metabolites had opposite effects on some of the GFP mutants in the two strains - BW and CSH4. For example, while addition of Malonate decreased fluorescence of C6 in CSH4, it increased the same mutant's fluorescence in BW (**Figure 6B, 6D**). Similar strain specific differences were obtained in different mutants of GFP in the presence of Betaine or Proline (**Figure 6B, 6D**). This is expected if the cellular metabolite pool participates in proteostasis and changes differently in presence of an excess metabolite depending upon the genetic background. Thus, alteration in metabolic states alters mutational buffering for the folding compromised mutants.

Taken together with our previous observation that these mutants are primarily dependent upon chemical chaperones for folding, we posit a prominent role of metabolism and metabolites in regulating differences in proteostasis capacity.

Osmotic compositions are able to determine the spectrum of mutational buffering

Is the link between metabolism and mutational buffering relevant in context of natural evolution? To answer, we checked if adaptation of an organism in a different niche (that changes

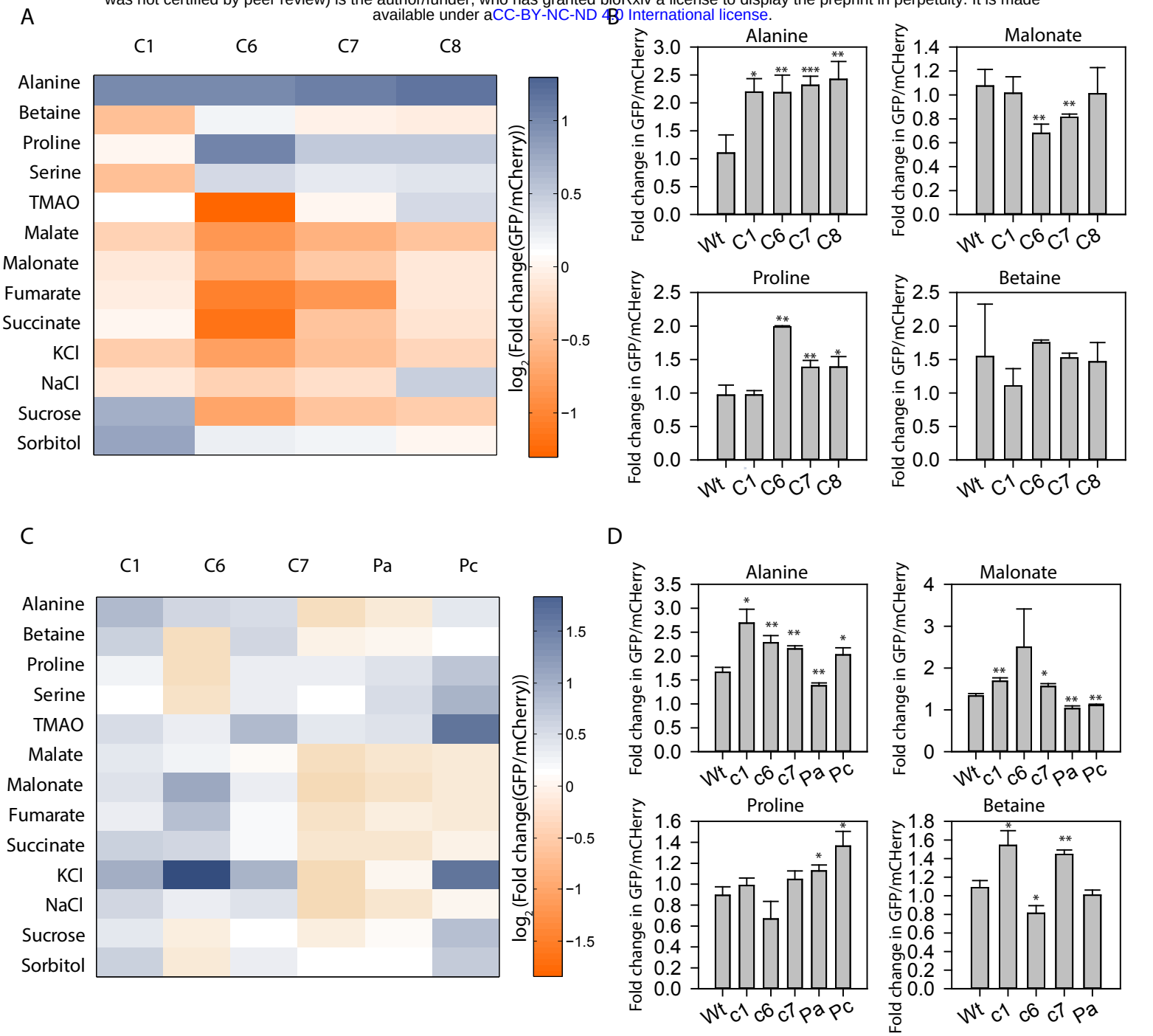

Figure 6: Altering cellular metabolism by exogenous supplementation of metabolites modifies mutational buffering capacity

A. Expression of Wt GFP and mutants were induced in CSH4 cells either growing in LB or in LB containing different metabolites. Median of GFP/mCherry fluorescence as measured by single-cell fluorescence is shown as heat map

B. Fold change in median of GFP/mCherry fluorescence in few metabolites (Alanine, Proline, Malonate, Betaine) is shown as bar graph along with standard deviations from three biological replicates and P-value calulated with respect to Wt by students's t-test.

C. Expression of Wt GFP and mutants were induced in BW cells either growing in LB or in LB containing different metabolites. Median of GFP/mCherry fluorescence as measured by single-cell fluorescence is shown as heat map

D. Fold change in median of GFP/mCherry fluorescence in BW when grown in LB added with Alanine, Proline, Malonate and Betaine is shown as bar graph along with standard deviations from three biological replicates and P-value calulated with respect to Wt by students's t-test.

metabolism) is associated with the evolution of an altered buffering capacity; we chose to evolve WT *E. coli* (BW25113) to adapt to high salt stress (**Figure 7A**). The strain was continuously passaged in LB in the presence of 500mM of NaCl. We kept the evolution duration short in order to ensure that drift mutations are minimal. Multiple strains were generated by parallel laboratory adaptive evolution, and we obtained strains that were fitter in the presence of osmotic stress by approximately 500 generations (**Figure 7B**). We argued that adaptation for growth in chronic hyperosmotic stress would have fixed mutations that perturb the osmotic composition and hence rewired the metabolic status of the cell. We confirmed that these strains indeed have difference in metabolite pool even when grown in the absence of osmotic shock (**Figure 7C**) we could now ask if these metabolic differences changed the mutational buffering capacity. Remarkably, the strains tested showed buffering specifically for the C1 and C7 mutants of GFP that were buffered in WG350 during osmotic stress (**Figure 7D**). The activities of the mutants were two to four fold higher in the different evolved strains in mutant-specific manner though the folding of Wt GFP was not altered in these strains (**Figure S5A, S5B**). However, *E.coli* molecular chaperones DnaK and GroEL were not upregulated in the evolved strains compared to the unevolved BW strain as checked by immunoblotting (**Figure 7E**) indicating that canonical hubs of proteostasis were not altered in these evolved strains. We confirmed by chase assay that degradation of the buffered mutants was indeed slower in strains that show buffering than in the unevolved strain (**Figure 7F, S5C**). We confirmed that slower degradation of these mutants in the evolved strain was independent of the activity of the degradation machinery as another degradation prone mutant of GFP (sGFP) degraded as rapidly in the evolved strain as in the unevolved strain (**Figure S5D**); impaired degradation hence is a fallout of faster folding of the buffered GFP mutants in the evolved strains. This indicated that a completely different strain evolved to have altered osmotic composition is able to buffer similar mutational variation as seen in the WG350 strain during osmotic shock. Response to osmotic shock, or a similar metabolic state once fixed in the genome in the absence of osmotic shock, is able to buffer similar mutational variations. Similar to GFP mutants, mutants of GmR also exhibited higher activity in most of evolved strains than the unevolved strain (**Figure 7G, H**). Importantly, each of the mutants had different activities in the different osmotolerant strains. Taken together the metabolic state of a cell is directly linked to their ability to buffer mutational variations. Adaptation to a niche with different osmolarity changes the spectrum of mutations buffered. This in turn could change the route of molecular

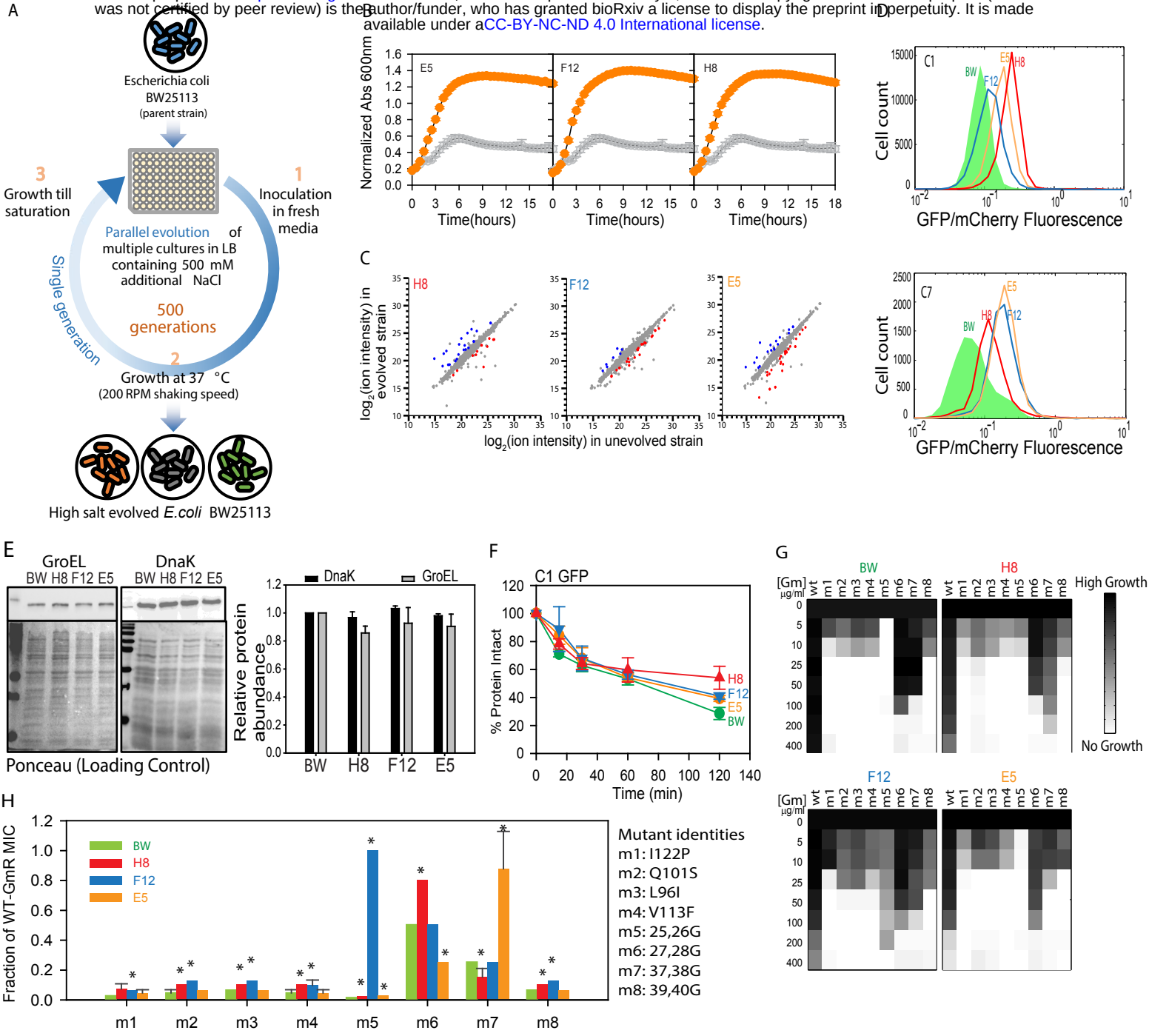

Figure 7: Wild-type cells evolve altered buffering capacity with evolution of a different metabolome

A.Schematic of strategy for Laboratory Adaptive Evolution of osmotolerant strains of *E. coli* starting from BW (WT *E. coli* K-12, BW25113).

B.Growth curve of evolved BW (WT *E. coli* K-12, BW25113) and osmotolerant strains E5, F12, H8 in 500mM of NaCl added in excess to LB medium while growing at 37°C, 200rpm.

C.Comparison of metabolite features of representative evolved strains (E5, F12 and H8) and its comparison with BW. The colored circled represent metabolites that are significantly altered in the evolved strains.

D.Histogram for GFP/mCherry fluorescence of GFP mutants C1 and C7 in the BW and evolved strains (E5, F12 and H8).

E.Comparative quantification of chaperone proteins DnaK and GroEL in BW and evolved strains (E5, F12 and H8) were done by immunoblotting with specific antibodies as described earlier. Quantification of the chaperone levels are shown as bar graphs. Error bars represent standard deviation of three replicate measurements (p-value>0.05).

F.Chloramphenicol based chase for checking protein degradation rates were performed in BW and evolved strains (E5, F12 and H8) as discussed earlier. The levels of C1 GFP at different time points are shown as a function of time in different strains.

G.Heatmap for growth based activity of Gm-R mutants and Wt Gm-R in unevolved strain (BW) and evolved strains (E5, F12 and H8) in increasing concentrations of gentamicin.

H.Bar graph representing percentage MIC of a selected set of Gm-R mutants w.r.t Wt Gm-R in the respective strains. Error bars represent standard deviation from 2 biological replicates.

Also see Figure S5.

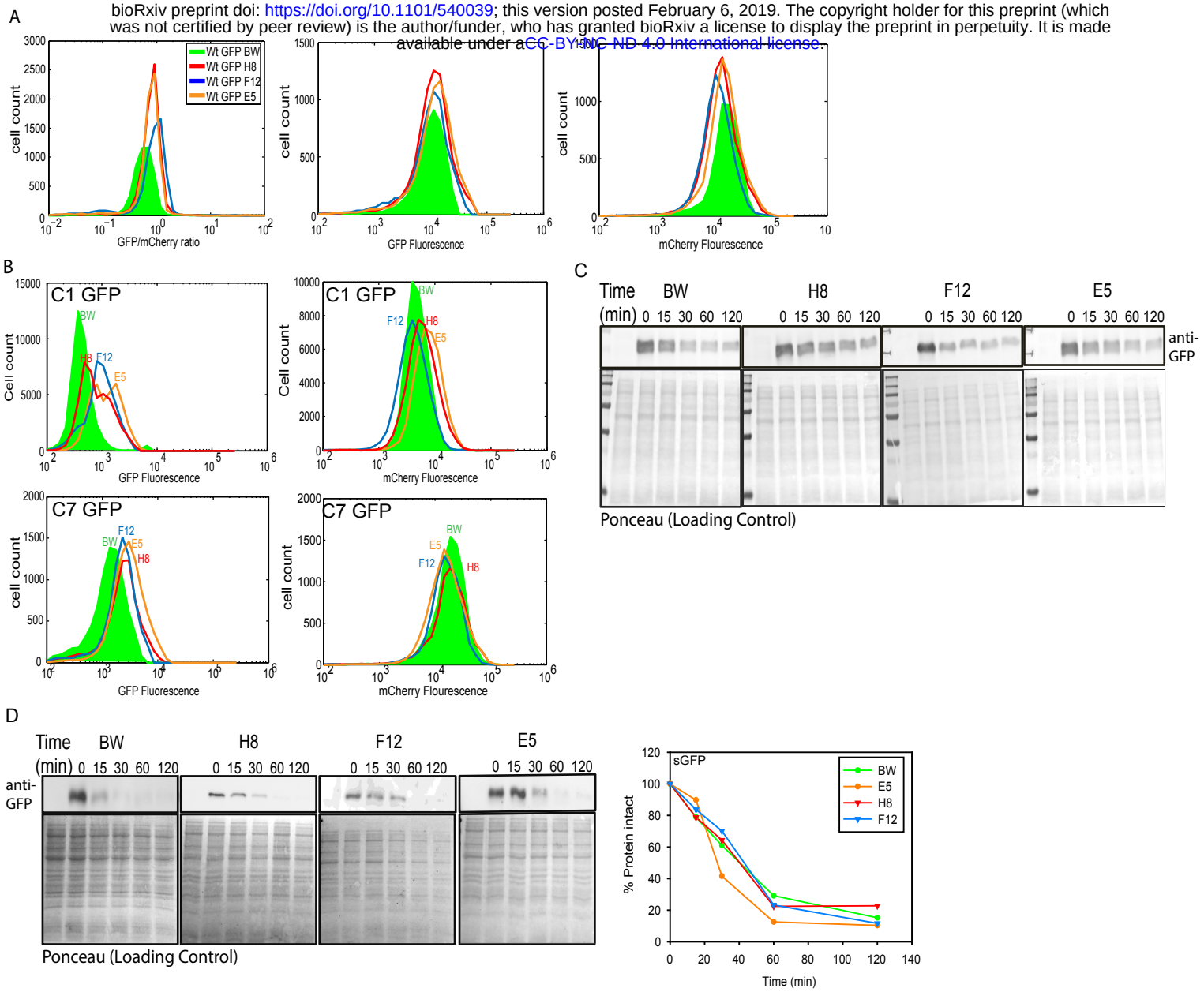

FIGURE S5: Modification in metabolome due to evolution changes the mutation buffering capacity of the cell (Related to Figure 7)

A. Histogram for Wt GFP fluorescence represented as ratio of GFP/mCherry fluorescence (left panel), GFP (middle panel) and mCherry fluorescence (right panel) in unevolved BW (WT E.coli K 12, BW25113) and evolved osmotolerant strains E5, F12, H8.

B. Histogram for fluorescence of GFP mutants C1 and C7 in GFP channel (left panels) and mCherry channel (right panels) in unevolved BW (WT E.coli K 12, BW25113) and evolved osmotolerant strains E5, F12, H8.

C. Representative images of Chloramphenicol based chase for checking degradation rates of C1 GFP in BW (WT E.coli K 12, BW25113) and evolved strains E5, F12, H8. GFP is degraded slower in evolved strains than BW

D. Representative images of Chloramphenicol based chase for sGFP in BW (WT E.coli K 12, BW25113) and evolved strains E5, F12, H8. sGFP is degraded with similar rates in evolved and unevolved BW

357 evolution of proteins, linking metabolism to evolution of protein sequences through alterations in
358 proteostasis.

359 **Implications**

360 In this work we have indicated the capability of *E. coli*, a prokaryotic unicellular organism, in
361 affecting mutational buffering through accumulation of small molecules in the cell. This, to the
362 best of our knowledge, is a maiden report that specifically describes the chaperoning activity of
363 the small molecule component of the cytosol of *E. coli*. While this fact is important, its
364 regulation through osmotic shock or genetic alterations makes it even more interesting in the
365 context of regulation of protein folding. Regulation of protein folding capacity enables condition
366 specific canalization or decanalization of mutants[46–48]. This we believe would be important when
367 organisms shift niches and evolve new functionalities. It is tempting to speculate that conditions
368 that have been reported to lead to altered Hsp90 levels during the evolution of *A. mexicanus* cave
369 dwelling variants, may also have led to alteration in intracellular osmolyte composition[51]. While
370 *E. coli* is a primitive model organism to comment on adaptive strategies and genetic buffering in
371 higher eukaryotes with complex developmental pathways, it surely paves way for more
372 interesting investigations to establish the potential link between osmotic composition, and their
373 alterations with canalization.

374 The work may also have important implications in explaining differences in the tissue-specificity
375 and late-onset nature in different aggregation associated diseases[52–55]. It is already well-known
376 that dietary restrictions or molecules like metformin that alters metabolism, assist
377 proteostasis[56,57]. While a large body of work has ascribed these beneficial effects on different
378 canonical proteostasis pathways like autophagy and ERAD[58–61], it is possible that altered cellular
379 milieu may contribute towards alleviating age-dependent proteostasis collapse[57]. Further
380 investigations would be required to test this relation.

381 Alteration of metabolic states, as shown in this work provides a new avenue for alteration of
382 proteostasis. Use of a simple model organism serves as an *in vivo* test tube to propose and test
383 the hypotheses related to cellular milieu. In our case we tested that composition of cellular milieu
384 alters with metabolism, and has the potential to alter protein folding and proteostasis network.
385 This may link metabolism to misfolding diseases and provide alternate routes to manipulate cells

386 to fold proteins more efficiently, in a case by case basis. We emphasize the importance of the
387 "case-by-case" part of the statement, as it is seen that while one metabolic state may allow better
388 folding of some mutants of a particular protein, it is not guaranteed to help other mutants of the
389 same protein or mutants of some other protein. It therefore needs to be considered carefully
390 whether there is anything like a better proteostasis than a physiological state, or it is simply an
391 altered state of proteostasis.

392 **Acknowledgement**

393 The work was done in KC Lab with the grant DST/SJF/LSA-01/2015-16 as Swarnajayanthi
394 Fellowship Grant from DST, and partly from BSC0124 from CSIR. Work in DS lab was funded
395 through BSC0124 project from CSIR. Instrument support was also obtained from Wellcome
396 Trust-DBT India Alliance (KC lab) and CSIR (DS, KC lab). KC acknowledges CSIR and CSIR-
397 IGIB for infrastructural support. KV, RD, AC, MR, ZZ acknowledge CSIR; KS and RD
398 acknowledge UGC; AS acknowledge ICMR, for fellowship support.

399

400 **Author Contribution**

401 Conceptualization: Kausik Chakraborty

402 Supervision: Kausik Chakraborty, Dhanasekaran Shanmugam

403 Reagent Generation: Kanika Verma, Kanika Saxena, Rajashekar Donaka

404 Experiments: Kanika Verma, Kanika Saxena, Rajashekar Donaka, Manish Rai, Aseem
405 Chaphalkar, Anurag Shukla, Zainab Zaidi

406 Analysis: Kanika Verma (FACS/Image/Metabolomics), Kanika Saxena (Mutant library
407 design/FACS), Anurag Shukla (Metabolomics), Manish Rai (Amplicon
408 sequencing/transcriptomics), Rohan Dandage (amplicon sequencing), Dhanasekhran
409 Shanmugam (metabolomics).

410 Manuscript writing: Kausik Chakraborty and Kanika Verma with inputs from all the authors. All
411 authors read and edited the manuscript.

412

413 **Declarations of Interest**

414 The authors declare no competing interests.

415

416 **References:**

417 1. Mallard, F., Nolte, V., Tobler, R., Kapun, M. & Schlötterer, C. A simple genetic basis of
418 adaptation to a novel thermal environment results in complex metabolic rewiring in
419 Drosophila. *Genome Biol.* **19,** (2018).

420 2. Maitra, A. & Dill, K. Bacterial growth laws reflect the evolutionary importance of energy
421 efficiency. *Proc Natl Acad Sci USA* **112,** 406–411 (2015).

422 3. Park, J. O. *et al.* Metabolite concentrations, fluxes, and free energies imply efficient
423 enzyme usage. *Nat. Chem. Biol.* **12,** 482–489 (2016).

424 4. Santra, M., Farrell, D. & Dill, K. Bacterial proteostasis balances energy and chaperone
425 utilization efficiently. *Proc Natl Acad Sci USA* **114,** E2654–E2661 (2017).

426 5. Yancey, P., Clark, M., Hand, S., Bowlus, R. & Somero, G. Living with water stress:
427 evolution of osmolyte systems. *Science (80-.).* **217,** 1214–1222 (1982).

428 6. Avanesov, A. S. *et al.* Age- and diet-associated metabolome remodeling characterizes the
429 aging process driven by damage accumulation. *Elife* **3,** (2014).

430 7. Diamant, S., Eliahu, N., Rosenthal, D. & Goloubinoff, P. Chemical Chaperones Regulate
431 Molecular Chaperones in Vitro and in Cells under Combined Salt and Heat Stresses. *J.*
432 *Biol. Chem.* **276,** 39586–39591 (2001).

433 8. Labbadia, J. *et al.* Cell Rep. **21,** 1481–1494 (2017).

434 9. Honda, Y., Tanaka, M. & Honda, S. Trehalose extends longevity in the nematode
435 Caenorhabditis elegans. *Aging Cell* **9,** 558–569 (2010).

436 10. Yerbury, J. J. *et al.* Walking the tightrope: Proteostasis and neurodegenerative disease.
437 *Journal of Neurochemistry* **137,** (2016).

438 11. Chiti, F. & Dobson, C. M. Protein Misfolding, Amyloid Formation, and Human Disease:
439 A Summary of Progress Over the Last Decade. *Annu. Rev. Biochem.* **86,** 27–68 (2017).

440 12. Chaveroux, C. *et al.* Nutrient shortage triggers the hexosamine biosynthetic pathway via
441 the GCN2-ATF4 signalling pathway. *Sci. Rep.* **6,** 27278 (2016).

442 13. Kandror, O., Bretschneider, N., Kreydin, E., Cavalieri, D. & Goldberg, A. L. Yeast Adapt
443 to Near-Freezing Temperatures by STRE/Msn2,4-Dependent Induction of Trehalose

444 Synthesis and Certain Molecular Chaperones. *Mol. Cell* **13,** 771–781 (2004).

445 14. Perić, M. *et al.* TORC1-mediated sensing of chaperone activity alters glucose metabolism
446 and extends lifespan. *Aging Cell* **16,** 994–1005 (2017).

447 15. Zhang, C.-S. *et al.* Fructose-1,6-bisphosphate and aldolase mediate glucose sensing by
448 AMPK. *Nature* (2017). doi:10.1038/nature23275

449 16. Bukau, B., Weissman, J. & Horwich, A. Molecular chaperones and protein quality control.
450 *Cell* **125,** 443–451 (2006).

451 17. Rabinowitz, J. D. & White, E. Autophagy and Metabolism. *Science (80-.).* **330,** 1344–
452 1348 (2010).

453 18. Suhm, T. *et al.* Mitochondrial Translation Efficiency Controls Cytoplasmic Protein
454 Homeostasis. *Cell Metab.* **27,** 1309–1322.e6 (2018).

455 19. Hartl, F. U. Molecular Chaperones in the Cytosol: from Nascent Chain to Folded Protein.
456 *Science (80-.).* **295,** 1852–1858 (2002).

457 20. Arsène, F., Tomoyasu, T. & Bukau, B. The heat shock response of Escherichia coli. *Int. J.*
458 *Food Microbiol.* **55,** 3–9 (2000).

459 21. Tokuriki, N. & Tawfik, D. S. Chaperonin overexpression promotes genetic variation and
460 enzyme evolution. *Nature* **459,** 668–673 (2009).

461 22. Farkas, Z. *et al.* Hsp70-associated chaperones have a critical role in buffering protein
462 production costs. *Elife* **7,** (2018).

463 23. Bukau, B. & Horwich, A. L. The Hsp70 and Hsp60 Chaperone Machines. *Cell* **92,** 351–
464 366 (1998).

465 24. Rutherford, S. L. Between genotype and phenotype: protein chaperones and evolvability.
466 *Nat. Rev. Genet.* **4,** 263–274 (2003).

467 25. Tomala, K. & Korona, R. Molecular chaperones and selection against mutations. *Biol.*
468 *Direct* **3,** 1–16 (2008).

469 26. Bandyopadhyay, A. *et al.* Chemical chaperones assist intracellular folding to buffer
470 mutational variations. *Nat. Chem. Biol.* **8,** 238–245 (2012).

471 27. Dandage, R. *et al.* Classification of chemical chaperones based on their effect on protein
472 folding landscapes. *ACS Chem. Biol.* **10,** 813–820 (2015).

473 28. Sévin, D. C., Stählin, J. N., Pollak, G. R., Kuehne, A. & Sauer, U. Global Metabolic
474 Responses to Salt Stress in Fifteen Species. *PLoS One* **11,** e0148888 (2016).

475 29. Yancey, P. H. Organic osmolytes as compatible, metabolic and counteracting
476 cytoprotectants in high osmolarity and other stresses. *J. Exp. Biol.* **208,** 2819–2830 (2005).

477 30. Bolen, D. . & Baskakov, I. V. The osmophobic effect: natural selection of a

thermodynamic force in protein folding 1 1Edited by D. Draper. *J. Mol. Biol.* **310,** 955–963 (2001).

31. Ignatova, Z. & Gierasch, L. M. Inhibition of protein aggregation in vitro and in vivo by a natural osmoprotectant. *Proc. Natl. Acad. Sci.* **103,** 13357–13361 (2006).

32. Nascimento, C., Leandro, J., Tavares de Almeida, I. & Leandro, P. Modulation of the Activity of Newly Synthesized Human Phenylalanine Hydroxylase Mutant Proteins by Low-Molecular-Weight Compounds. *Protein J.* **27,** 392–400 (2008).

33. Schultz, T., Liu, J., Capasso, P. & Marco, A. de. The solubility of recombinant proteins expressed in Escherichia coli is increased by otsA and otsB co-transformation. *Biochem. Biophys. Res. Commun.* **355,** 234–239 (2007).

34. Wolf, E. *et al.* Crystal Structure of a GCN5-Related N-acetyltransferase: Serratia marcescens Aminoglycoside 3-N-acetyltransferase. *Cell* **94,** 439–449 (1998).

35. Cormack, B. P. *et al.* Yeast-enhanced green fluorescent protein (yEGFP): a reporter of gene expression in Candida albicans. *Microbiology* **143,** 303–311 (1997).

36. Dandage, R. *et al.* Differential strengths of molecular determinants guide environment specific mutational fates. *PLoS Genet.* **14,** (2018).

37. Newton, W. A., Beckwith, J. R., Zipser, D. & Brenner, S. Nonsense mutants and polarity in the lac operon of Escherichia coli. *J. Mol. Biol.* **14,** 290–6 (1965).

38. Culham, D. E. *et al.* Isolation and Sequencing of Escherichia coli Gene proP Reveals Unusual Structural Features of the Osmoregulatory Proline/Betaine transporter, ProP. *J. Mol. Biol.* **229,** 268–276 (1993).

39. Maurizi, M. R. Proteases and protein degradation inEscherichia coli. *Experientia* **48,** 178–201 (1992).

40. Baba, T. *et al.* Construction of Escherichia coli K-12 in-frame, single-gene knockout mutants: the Keio collection. *Mol. Syst. Biol.* **2,** 2006.0008 (2006).

41. Straus, D. B., Walter, W. A. & Gross, C. A. The heat shock response of E. coli is regulated by changes in the concentration of σ32. *Nature* **329,** 348–351 (1987).

42. Membrillo-Herna´ndez, J., Herna´ndez, H., Kim, S. O., Cook, G. M. & Poole, R. K. *Paraquat Regulation of hmp (Flavohemoglobin) Gene Expression in Escherichia coli K-12 Is SoxRS Independent but Modulated by sigma S. JOURNAL OF BACTERIOLOGY* **179,** (1997).

43. Breunig, J. S., Hackett, S. R., Rabinowitz, J. D. & Kruglyak, L. Genetic Basis of Metabolome Variation in Yeast. *PLoS Genet.* **10,** e1004142 (2014).

44. Mü, M. *et al.* Functional Metabolomics Describes the Yeast Biosynthetic Regulome. *Cell* **167,** 553–565 (2016).

45. Alam, M. T. *et al.* The metabolic background is a global player in Saccharomyces gene

514 expression epistasis. *Nat. Microbiol.* **1,** 15030 (2016).

515 46. Jarosz, D. F., Taipale, M. & Lindquist, S. Protein Homeostasis and the Phenotypic
516 Manifestation of Genetic Diversity: Principles and Mechanisms. **44,** 189–216 (2010).

517 47. Milton, C. C., Ulane, C. M. & Rutherford, S. Control of Canalization and Evolvability by
518 Hsp90. *PLoS One* **1,** e75 (2006).

519 48. Zabinsky, R. A., Mason, G. A., Queitsch, C. & Jarosz, D. F. It's not magic – Hsp90 and
520 its effects on genetic and epigenetic variation. *Semin. Cell Dev. Biol.* (2018).
521 doi:10.1016/J.SEMCDB.2018.05.015

522 49. Milton, C. C., Ulane, C. M. & Rutherford, S. Control of canalization and evolvability by
523 Hsp90. *PLoS One* **1,** e75 (2006).

524 50. Geiler-Samerotte, K., Sartori, F. M. O. & Siegal, M. L. Decanalizing thinking on genetic
525 canalization. *Semin. Cell Dev. Biol.* **doi:10.101,** (2018).

526 51. Rohner, N. *et al.* Cryptic variation in morphological evolution: HSP90 as a capacitor for
527 loss of eyes in cavefish. *Science* **342,** 1372–5 (2013).

528 52. Federici, F., Dupuy, L., Laplaze, L., Heisler, M. & Haseloff, J. Integrated genetic and
529 computation methods for in planta cytometry. *Nat. Methods* **9,** 483–485 (2012).

530 53. Brehme, M. *et al.* A Chaperome Subnetwork Safeguards Proteostasis in Aging and
531 Neurodegenerative Disease. *Cell Rep.* **9,** 1135–1150 (2014).

532 54. Sala, A. J., Bott, L. C. & Morimoto, R. I. Shaping proteostasis at the cellular, tissue, and
533 organismal level. *Journal of Cell Biology* 1231–1241 (2017). doi:10.1083/jcb.201612111

534 55. Ben-Zvi, A., Miller, E. A. & Morimoto, R. I. Collapse of proteostasis represents an early
535 molecular event in Caenorhabditis elegans aging. *Proc. Natl. Acad. Sci.* **106,** 14914–
536 14919 (2009).

537 56. Dai, S. *et al.* Suppression of the HSF1-mediated proteotoxic stress response by the
538 metabolic stress sensor AMPK. *EMBO J.* **34,** 275–93 (2015).

539 57. Taylor, R. C. & Dillin, A. Aging as an event of proteostasis collapse. *Cold Spring Harb.*
540 *Perspect. Biol.* **3,** a004440 (2011).

541 58. Vilchez, D., Saez, I. & Dillin, A. The role of protein clearance mechanisms in organismal
542 ageing and age-related diseases. *Nat. Commun.* **5,** 5659 (2014).

543 59. Koyuncu, S. *et al.* The ubiquitin ligase UBR5 suppresses proteostasis collapse in
544 pluripotent stem cells from Huntington's disease patients. *Nat. Commun.* **9,** 1–22 (2018).

545 60. Kaushik, S. & Cuervo, A. M. Proteostasis and aging. *Nat. Med.* **21,** 1406–1415 (2015).

546 61. Gamerdinger, M. *et al.* Protein quality control during aging involves recruitment of the
547 macroautophagy pathway by BAG3. *EMBO J.* **28,** 889–901 (2009).

548 62. Bolger, A. M., Lohse, M. & Usadel, B. Genome analysis Trimmomatic: a flexible trimmer
549 for Illumina sequence data. **30,** 2114–2120 (2014).

550 63. Bray, N. L., Pimentel, H., Melsted, P. & Pachter, L. Near-optimal probabilistic RNA-seq
551 quantification. *Nat. Biotechnol.* **34,** 525–527 (2016).

552 64. Zhang, C., Zhang, B., Lin, L.-L. & Zhao, S. Evaluation and comparison of computational
553 tools for RNA-seq isoform quantification. doi:10.1186/s12864-017-4002-1

554 65. Leng, N. *et al.* Gene expression EBSeq: an empirical Bayes hierarchical model for
555 inference in RNA-seq experiments. **29,** 1035–1043 (2013).

556 66. Clasquin, M. F., Melamud, E. & Rabinowitz, J. D. LC-MS data processing with MAVEN:
557 a metabolomic analysis and visualization engine. *Curr. Protoc. Bioinforma.* **Chapter 14,**
558 Unit14.11 (2012).

559 67. Lu, W. *et al.* Metabolomic analysis via reversed-phase ion-pairing liquid chromatography
560 coupled to a stand alone orbitrap mass spectrometer. *Anal. Chem.* **82,** 3212–21 (2010).

561 68. Castanié, M.-P., Bergès, H., Oreglia, J., Prère, M.-F. & Fayet, O. A Set of pBR322-
562 Compatible Plasmids Allowing the Testing of Chaperone-Assisted Folding of Proteins
563 Overexpressed inEscherichia coli. *Anal. Biochem.* **254,** 150–152 (1997).

564 69. Tiwari, S., Kumar, V., Jayaraj, G. G., Maiti, S. & Mapa, K. Unique Structural Modulation
565 of a Non-Native Substrate by Cochaperone DnaJ. *Biochemistry* **52,** 1011–1018 (2013).

566 70. Brown, K. M., Donohue, D. E., D'Alessandro, G. & Ascoli, G. A. A Cross-Platform
567 Freeware Tool for Digital Reconstruction of Neuronal Arborizations From Image Stacks.
568 *Neuroinformatics* **3,** 343–360 (2005).

569 71. Smith, C. A., Want, E. J., O'Maille, G., Abagyan, R. & Siuzdak, G. XCMS: Processing
570 mass spectrometry data for metabolite profiling using nonlinear peak alignment, matching,
571 and identification. *Anal. Chem.* **78,** 779–787 (2006).

572 72. Silva, R. R. *et al.* ProbMetab: An R package for Bayesian probabilistic annotation of LC-
573 MS-based metabolomics. *Bioinformatics* **30,** 1336–1337 (2014).

574 73. Yang, F., Moss, L. G. & Phillips, G. N. The molecular structure of green fluorescent
575 protein. *Nat. Biotechnol.* **14,** 1246–1251 (1996).

576

577

578

579 **TABLES**

580 None

581

582

METHODS

EXPERIMENTAL MODEL AND SUBJECT DETAILS

Strains, Plasmids and Proteins

E. coli strain DH5α was used for cloning, WT *E. coli* (K-12 BW25113 referred to as BW) strains was used for expression of arabinose inducible pBAD GFP mCherry and BL21 (DE3) was used for protein expression and purification. Protein concentrations were determined spectrophometrically at 562 nm using BCA kit (Pierce ThermoFisher Scientific). Deletion strains were obtained from CGSC as part of Keio collection {Baba, 2006 #1843}.

METHOD DETAILS

Construction of mutant GFP mutant library

Mutant GFP library was made in arabinose inducible pBAD vector using random mutagenesis approach. In the 1st step YeGFP (referred to as GFP) was amplified using GFP specific primers and Mutazyme II polymerase (Agilent Technologies; Cat no.: 200550) in order to incorporate 7-11 mutations per kb of plasmid. In the 2nd step, the product of 1stamplification was used as mega-primer to amplify the entire plasmid with Wt GFP (pBAD GFP mCherry) as template using Kapa Biosystems Hifi readymix (NC02955239) for 25 cycles with both annealing and extension at 72^{O}C. The Wt copy of plasmid was digested with DpnI followed by transformation of chemically competent DH5α cells. The colonies were scraped and plasmid was prepared in pool to yield library of GFP mutants. The said library has a total complexity of around 10,000 mutations. The reporter is constructed such that GFP and mCherry are under same arabinose inducible pBAD promoter in an operon to give readout of GFP according to the mutation created on it but the mCherry readout will remain similar thus serving as an internal control for transcription, translation and inducibility.

Screening of mutant GFP library for folding mutants responsive to osmotic stress

Wild type *E.coli* cells (BW) were transformed with mutant GFP library maintaining 10 fold converge for preserving complexity. Cells were induced with 0.1% arabinose at the time of inoculation and fluorescence was observed on BD LSR II five hours post induction at 37^{O}C after diluting cells in 1X PBS and incubating at 37^{O}C for 1 hour. Fluorescence of the mutant library was studied in a pooled manner against wild type GFP. The entire library was sorted using BD

Aria III into populations of compromised mutants (low fluorescent) and active mutants (high fluorescent) according to the GFP fluorescence. Each of these populations was purified and plasmids prepared. CSH4 and WG350 strains were transformed with the purified populations and subjected to osmotic stress with 350mM NaCl. The pool of mutants buffered under osmotic stress in WG350 was sorted and single clones of GFP were picked from here and checked for their fluorescence in presence and absence of osmotic stress. The isolated mutants having higher fluorescence in WG350 under osmotic stress were identified by Sanger's sequencing, also cloned in pET SUMO under BamHI and HindIII restriction sites and purified using *E. coli* BL21 (DE3) for further characterization.

Growth curve

Single colony of *E.coli* cells were inoculated in LB and grown overnight at 37^{O}C, 200 rpm. Secondary inoculations were done in LB (control) and LB containing 350mM, 500mM NaCl additional in honey comb plates with temperature maintained at 37^{O}C, 200 rpm shaking. Absorbance at 600nm was measured every 30 minutes using Bioscreen C (Oy growth curve Ab Ltd).

Transcriptomics

3 ml of overnight grown culture in LB at 37^{O}C from a single colony was used to re-inoculate at 0.1% culture in 10 ml of LB and grown till OD600 reaches 0.5. The culture was mixed with equal volume of bacteria RNA protect reagent followed by RNA isolation using Qiagen RNeasy Mini Kit and TURBO DNA-free kit (AM1907). Quality of RNA was checked using RNA 600 Nano bioanalyzer kit and MICROB Express bacterial mRNA enrichment kit (AM1905) was used to remove rRNA. 100 ng RNA was used to prepare library using Ion Total RNA-seq kit V2 (4475936) and Ion Xpress RNA-seq barcode 1-16 kit. Final quality check and quantification were done using DNA HS bioanalyzer (5067-4626) and qubit HS DNA kit (Q32854). Equal amount of each sample was pooled followed by emulsion PCR (Ion PI Hi-Q OT2 200) and sequencing (Ion PI Hi-Q sequencing 200 kit) FastQC- tool kit was used for Data QC followed by Trimmomatic [62] to remove low quality reads. TPM was calculated using Kallisto (Zhang *et al.*, 2017; Bray *et al.*, 2016) followed by identification of differentially expressed genes using EB sequencing analysis pipeline(https://bioconductor.org/packages/release/bioc/html/EBSeq.html)[65].

Metabolomics

3ml of LB was inoculated with 0.1% inoculum from overnight grown culture and grown till OD600~0.8 at 37^{O}C, 200 rpm. Cells equivalent to 0.1 OD were harvested at 14000 rpm, 1 min, 4^{O}C. Supernatant was discarded and 200ul 80% chilled methanol (80% MetOH, PIPES 1ng/µl, U13C-U15N-glutamine in MS grade water) was added to the pellet and incubated in ice for 5 minutes for quenching. This is followed by sonication in water bath for 15 min at 4^{O}C with intermittent vortexing. Metabolites were collected in the supernatant by centrifugation at 14000 rpm for 1 min at 4^{O}C. Previous step was repeated twice by adding 100µl 80% chilled methanol each time to increase metabolite yield and stored in -80 refrigerator till further analysis. The untargeted mass profile (or metabolic profile) was acquired in Thermo Q-exactive Orbitrap coupled with Thermo Accucore RP C18 150*2.1, 2.6µM column with flow rate of 200µl/min. Ion masses from 80-1000m/z were collected in negative ion mode. The raw output files obtained from mass spec were converted into .mzXML files using proteowizard tool (http://proteowizard.sourceforge.net/) followed by identification and analysis using metabolomics data processing software platformXCMS and MAVEN(http://genomics-pubs.princeton.edu/mzroll/index.php?show=index)[66,67].

Minimum Inhibitory Concentration (MIC) study of Gm-R glycine doublet mutants

The library of Gm-R glycine doublet mutants as reported previously (Bandyopadhyay *et al*., 2012) were grown overnight in LB containing ampicillin(100µg/ml) and Arabinose(0.1%) at 37^{O}C, 200 rpm. Secondary inoculations were done in LB containing Ampicillin(100µg/ml), Arabinose(0.1%) and increasing concentrations of gentamicin (0-800 µg/ml) incubated for 16hrs at 37^{O}C and 200rpm. Growth was assessed by measuring absorbance at 600nm in flat bottom 96 well microtiter plate using TECAN infinite 200 pro. Absorbance value for each sample under selection pressure by gentamicin was normalized against absorbance of respective unselected sample. To check for mutation specific effects it was important to normalize for the growth differences of Wt-GmR transformed in the different strains that were being compared. To obtain a semi-quantitative indication for activity of the different mutants, wt-GmR transformed cells was grown as control, and the MIC for the mutants were normalized with respect to the MIC of wt-GmR in the same strains. This allowed us to obtain mutation-specific effects in activity in the different strains used.

676 **Amplicon sequencing**

677 Plasmids were isolated from unselected (no gentamicin) and selected cells under gentamicin
678 selection pressure. Gm-R gene was amplified for 25 cycles using Kapa Hifi Hotstart polymerase.
679 The 500bp amplicons were gel purified and quantified using qubit. 150ng of purified products
680 was used for library preparation Ion Plus Fragment Library Kit (part no.-4471252) and Ion
681 Xpress Barcode Adapters (4471250, 4474009). The final library was quantified and equal
682 amount of DNA library of 8 samples were pooled and emulsion PCR and sequenced using Ion
683 PGM Hi-Q OT2 Kit (part no A29900) and Ion PGM Hi-Q sequencing kit (part no.A30044) on
684 Ion Torrent platform. Analysis was done using FastqQC followed by trimmomatic (cutoff Q15)
685 and quality check by fastQC. Good reads were aligned to Gm-R gene followed by variant calling
686 and fitness score calculation www.github.com/kc-lab/dms2dfe[36].
687
688 **Qunatitation of activity of Gm-R Glycine-doublet substitution mutants**
689 To obtain a measure for activity of the mutants, we obtained the read count for each of the
690 mutant and normalized with respect to the coverage at the respective positions. The relative read-
691 counts of the mutants did not differ between the different strains in the absence of any selection
692 pressure for GmR indicating that the library was homogeneously covered in all the
693 transformations. We thereby did not obtain relative enrichment but compared the coverage-
694 normalized read-counts between the different strains and conditions to obtain differences in
695 activity. All the amplicon based sequencing experiments were done in duplicates.
696 To obtain relative activity of the different mutants in one strain (for comparison of activity of
697 mutants as measured by amplicon sequencing and MIC assay as shown in Figure S1E) we
698 obtained the enrichment score for each mutant by dividing the normalized read count for each
699 mutant with Gm selection and in the absence of Gm-selection. z-scores were obtained for each of
700 the mutant assuming a normal distribution. A positive z-score indicates higher than average
701 activity while a negative z-score indicated a lower than average activity. Mutants were picked
702 that had a high z-score (1.4, more active than average) or low z-score (-1.6 less active than
703 average) or one close to zero (z-score = -0.4, activity close to average) for checking the MICs.
704 Note: z-score was not used to obtain the significance of difference but the mutants that exhibited
705 either high or low activity.
706

Chase for degradation of protein

From overnight grown culture in LB containing Ampicillin(100µg/ml) secondary cultures were inoculated with 0.1% inoculum in 100 ml LB containing Ampicillin(100µg/ml) and grown till OD600 reached 0.5. Cells were harvested and resuspended in 10ml of the spent media. GFP was induced using 0.5% arabinose for 5 minutes at 37^{O}C and 200 rpm. Chloramphenicol (50µg/ml) was used to arrest translation. 1 ml of culture was taken out for uninduced, 0 min, 15 min, 30 min, 60 min, 120 min post translation arrest, harvested, snap chilled and protein was collected by lysing cells resuspended in 1X PBS using 2X lysis buffer (Tris pH 6.8(80mM), SDS 1%, glycerol 10%). 30µg of protein estimated using Pierce™ BCA Protein Assay Kit and loaded on SDS-PAGE followed by Western blotting probing for GFP using Rabbit anti-GFP (Ab290) and HRP conjugated goat anti-rabbit IgG (SantaCruz Biotechnology).

***In-vivo* crosslinking:**

100ml of LB medium (with and without 350mM of NaCl) containing Ampicillin (100µg/ml) was inoculated with overnight grown cells at 0.1% inoculum for each strain. Cells were grown till they reach $O.D_{600}$ 0.5 and harvested at 4000 rpm for 10 mins at RT. Pellet was finally resuspended in 2ml of spent media and induced for 5 minutes at 37^{O}C with 0.5% arabinose for GFPexpression. Cells were harvested and resuspended in 2 ml of 1X PBS containing protease inhibitor cocktail (Roche) and 500µl of resuspended cells was taken as a control for uncrosslinked sample (referred to as -DSG in the text). To the remaining cells, 300µM of Di (N-succinimidyl) glutarate (DSG) was added and incubated at 37^{O}C for 10 minutes for crosslinking. Reaction was quenched with 100mM of Tris, pH 8 for 5-10 minutes at room temperature. Cells were harvested at 13000 rpm, 2 minutes at room temperature and lysed by Freeze-thaw method in the presence of protease inhibitors. 30µg of protein was loaded on SDS PAGE followed by Western Blotting.

Western Blotting Experiment

E. coli cells were inoculated in LB and grown at 37^{O}C for five hours. Cells were harvested and resuspended in 1X PBS (Himedia; ML023). Equal volume of 2X lysis buffer was added and boiled at 95^{O}C for 15 minutes followed by spin at highest rpm for 15 minutes. The supernatant was collected and estimated for the amount of protein. 30µg of protein was used for SDS-PAGE

and Western Blotting post transferring onto nitrocellulose membrane (Millipore; HATF00010). The blots were decorated with antibodies against GroEL (Enzo; 9A1/2) and DnaK (Enzo; 9E2/2) isolated from mouse. Blots were developed using HRP conjugated Goat anti-mouse IgG (Genscript) and Luminata crescendo (Millipore). Densitometric analysis was done using ImageJ. (Rasband, W.S., ImageJ, U. S. National Institutes of Health, Bethesda, Maryland, USA, http://imagej.nih.gov/ij/, 1997-2011).

GFP refolding assay

60μM native GFP (or mutant) was mixed with 8M GuHCl prepared in GFP refolding buffer (Buffer-A) (Tris-Cl (25 mM), KCl (150mM), $MgCl_2$ (10mM), pH 7.4) in 1:3 ratio. After incubation at 25°C for 1 hour, refolding of GFP was initiated in Buffer-A by diluting the mixture 100 fold (final GFP concentration 150 nM). Real time fluorescence of GFP was monitored in Fluorolog 3 spectrophotometer (Horiba Jobin Yvon, with operating software FluorEssence v3.0) at 25°C, with excitation wavelength 488 nm (2 nm slit width) and emission wavelength 515 nm (5nm slit width), enabling 'anti-photobleaching' mode.The data acquired from refolding assays was analysed in OriginPro 8 (OriginLabcorporation).

Isolation of protein free cell extract

E. coli K12 (BW35113) strain was grown in 5 ml LB broth at 37°C, 200 RPM orbital shaking for overnight and this primary culture was used to inoculate a 500 ml secondary culture in LB broth. After growing the secondary culture in identical conditions for 3 hours (OD 0.7-0.8), the culture was centrifuged at 4000 RPM for 30 minutes at 37°C. 5 ml of boiling hot ultrapure water was added directly to the pellet, resuspending it vigorously, and the cell suspension was immediately collected in a glass test tube. The glass tube was kept in a boiling water bath for 30 minutes, ensuring maximum lysis of cells and precipitation of proteins. The resulting suspension was cooled down to room temperature and was centrifuged at 13000 RPM for 20 minutes. Absence of protein in the supernatant, the protein free cell extract, was confirmed by Bradford protein estimation assay.

768 **Simulation**

769 Numerical simulations was performed using the ODEs defined in Figure S3 to model a basic
770 framework to check the apparent rate of degradation as a function of folding rate in vivo. The
771 simulation was set up with 1000μM S (pool of DNA/RNA that is competent to make proteins). S
772 can form U (nascent polypeptides) with an overall unimolecular rate constant of ktrans (a
773 simplistic combination of rates of transcription and translation). The pool of U can either convert
774 to F (folded GFP) or be degraded with the unimolecular rate constants of k_f and k_{deg},
775 respectively. The pool of S can be blocked by I (inhibitor of translation) with a rate constant of
776 k_I. This was included to mimic translation arrest by chloramphenicol. The simulation was run in
777 the absence of I for 300 seconds. Following this, 1mM of I was dosed into the simulation to
778 rapidly quench S. Following this we monitored the total concentration of uncleaved GFP (U+F)
779 over time to mimic the results obtained from the chase experiments performed with anti-GFP
780 antibodies.

781

782 **QUANTIFICATION AND STATISTICAL ANALYSIS**

783 Student's t test and R package for non linear regression was used for statistical analysis. Flow-
784 cytometry data was analyzed using octave

785 **DATA AND SOFTWARE AVAILABILITY**

786 All data are provided in the manuscript. We did not develop any new software.

787

788

789 **KEY RESOURCES TABLE**

REAGENT	SOURCE	IDENTIFIE
Antibodies		
Anti GroEL (E.coli) mouse monoclonal	ENZO	9A1/2
Anti DnaK (E.coli) mouse monoclonal	ENZO	8E2/2
Anti DnaJ (E.coli) rabbit polyclonal	ENZO	SPA410
Anti Tig (E.coli) rabbit polyclonal	Genescript	A01329
Anti GFP rabbit polyclonal	Abcam	Ab290
Anti RecA rabbit polyclonal	Abcam	Ab125096
Anti Mouse secondary	Santa Cruz Biotechnology	SC2005
Anti rabbit secondary	Santa Cruz Biotechnology	SC2030
Di(N-succinimidyl) glutarate (DSG)	Sigma	80424
Bacterial and Virus Strains		
E.coli BL21 (DE3)		
E.coli DH5α		
BW (*E.coli* K12, BW25113) F-, DE(araD-araB)567, lacZ4787(del)::rrnB-3, LAM-, rph-1, DE(rhaD-rhaB)568, hsdR514	(Baba *et al.*, 2006)	CGSC#: 7636
Δ*Tig* (JW0426-1) *F-, Δ(araD-araB)567, ΔlacZ4787(::rrnB-3), Δtig-722::kan, λ-, rph-1, Δ(rhaD-rhaB)568, hsdR514*	(Baba *et al.*, 2006)	CGSC#: 8589
Δ*dnaK (*JW0013-4) F-, Δ(araD-araB)567, ΔlacZ4787(::rrnB-3), λ-, rph-1, ΔdnaK734::kan, Δ(rhaD-rhaB)568, hsdR514	(Baba *et al.*, 2006)	CGSC#: 8342
Δ*dnaJ (*JW0014-1) F-, Δ(araD-araB)567, ΔlacZ4787(::rrnB-3), λ-,rph-1, ΔdnaJ735::kan,Δ(rhaD-rhaB)568, hsdR514	(Baba *et al.*, 2006)	CGSC#: 8343
ΔclpA F-, Δ(araD-araB)567, ΔlacZ4787(::rrnB-3), λ-, ΔclpA783::kan,rph-1, Δ(rhaD-rhaB)568, hsdR514	(Baba *et al.*, 2006)	CGSC#: 8898
ΔclpP F-, Δ(araD-araB)567, ΔlacZ4787(::rrnB-3), ΔclpP723::kan, λ-,rph-1, Δ(rhaD-rhaB)568, hsdR514	(Baba *et al.*, 2006)	CGSC#: 8590
ΔclpX F-, Δ(araD-araB)567, ΔlacZ4787(::rrnB-3), ΔclpX724::kan, λ-, rph-1,Δ(rhaD-rhaB)568, hsdR514	(Baba *et al.*, 2006)	CGSC#: 8591
ΔhslU F-, Δ(araD-araB)567, ΔlacZ4787(::rrnB-3), λ-, rph-1, Δ(rhaD-rhaB)568, ΔhslU790::kan, hsdR514	(Baba *et al.*, 2006)	CGSC#: 10817

ΔhslV F-, Δ(araD-araB)567, ΔlacZ4787(::rrnB-3), λ-, rph-1, Δ(rhaD-rhaB)568, ΔhslV720::kan, hsdR514	(Baba *et al.*, 2006)	CGSC#: 10818
ΔsecB F-, Δ(araD-araB)567, ΔlacZ4787(::rrnB-3), λ-, ΔsecB721::kan, rph-1, Δ(rhaD-rhaB)568, hsdR514	(Baba *et al.*, 2006)	CGSC#: 10640
CSH4 F, lacZ1125, λtrpA49(Am), relA1, rpsL150(strR), spoT	(Newton *et al.*, 1965)	CGSC#: 8196
WG350 F-, lacZ1125, λ⁻, Δ(putA-putP)101, trpA49(Am), ΔproU-600, relA1, rpsL150(strR), spoT1, Δ(proP-melB)212	(Culham *et al.*, 1993)	CGSC#: 8195
Oligonucleotides		
GFP Forward primer (to clone in pET SUMO) CCCGGATCCATGTCTAAAGGTGAAGAATTATTCACTGGTGTTGTCCC	This Paper	
GFP Reverse primer (to clone in pET SUMO) CCCAAGCTTTTATTTGTACAATTCATCCATACCATGGGTAATA	This Paper	
GFP Forward primer (to clone in pBAD vector) TGTGCTGAATTCACATATATGTCTAAAGGTGAAGAATTATTCA	This Paper	
GFP Reverse primer (to clone in pBAD vector) ACGGCCAAGCTTTTATTTGTACAATTCATCCATACCATGGG	This Paper	
RBS mCherry Forward primer (to clone in pBAD vector) ACAAAGCTTTCCATACCCGTTTTTTGGGCTAACAGGAGGAATTAACCATGGTGA	This Paper	
RBS mCherry Reverse primer (to clone in pBAD vector) TCTAAGCTTCTACTTGTACAGCTCGTC	This Paper	
Recombinant DNA		
pOFX ELES (pOFX tac-SL2)	(Castanié *et al.*, 1997)	
pOFX DnaK/J/GrpE (pOFX tac-KJE1)	(Castanié *et al.*, 1997)	
pET duet1 dnaK	(Tiwari *et al.*, 2013)	
pET duet1 dnaJ	(Tiwari *et al.*, 2013)	
pET duet1 grpE	(Tiwari *et al.*, 2013)	
pET duet1 Mge1	(Tiwari *et al.*, 2013)	
pET SUMO sGFP	Sadat & Mapa (in process)	
pBAD GmR	(Bandyopadhyay *et al.*, 2012)	
pBAD 25G GmR	This Paper	
pBAD 27G GmR	This Paper	

pBAD 37G GmR	This Paper	
pBAD 39G GmR	This Paper	
pET SUMO c1GFP	This Paper	
pET SUMO c6FP	This Paper	
pET SUMO c7GFP	This Paper	
pET SUMO c8GFP	This Paper	
pBAD GFP mCherry	This Paper	
pBAD c1GFP mCherry	This Paper	
pBAD c6GFP mCherry	This Paper	
pBAD c7GFP mCherry	This Paper	
pBAD c8GFP mCherry	This Paper	
Software and Algorithms		
Chimera		
Proteowizard	(Brown *et al.*, 2005)	
XCMS	(Smith *et al.*, 2006; Silva *et al.*, 2014)	
Maven	(Lu *et al.*, 2010; Clasquin, Melamud and Rabinowitz, 2012)	
FastQC	http://www.citeulike.org/user/nailest/author/Andrews:S	
Trimmomatic	(Bolger, Lohse and Usadel, 2014)	
Kallisto	(Zhang *et al.*, 2017; Bray *et al.*, 2016)	
EBseq	(Leng *et al.*, 2013)	
ImageJ		
Origin Pro8		
Deposited Data		

790

Table S1: List of metabolites along with their log_2 of fold change and p- values obtained by untargeted metabolite profiling and analysis using MAVEN platform (Related to Figure 1 and 2)

S.no.	medMz	medRt	Max Quality	compound	Log_2 fold change				Log_{10} p-value			
					CSH4 - WG350	CSH4 - CSH4 (S)	WG350 - WG350 (S)	CSH4 (S)- WG350 (S)	CSH4-WG350	CSH4-CSH4 (S)	WG350-WG350 (S)	CSH4 (S)- WG350 (S)
1	363.0344	2.041682	0.848391	N-Acetylputrescine	0.00	-14.03	-14.29	-0.26	0.01	0.97	1.54	0.45
2	283.0684	4.029608	0.849596	Geranyl-PP	0.00	-13.99	-13.89	0.10	0.05	1.67	1.43	0.20
3	151.025	1.858412	0.819399	fructose-1-6-bisphosphate	0.00	-12.65	0.00	12.65	0.00	2.24	0.43	5.16
4	116.0705	2.341379	0.828605	succinate	0.00	-11.67	-25.78	-14.11	0.43	1.60	2.15	1.80
5	243.0622	2.131804	0.848934	UMP	2.10	-4.63	-4.86	1.87	0.49	2.56	1.80	1.80
6	167.0204	2.374183	0.847362	orotidine-5--phosphate	10.98	-4.25	-14.62	0.61	1.12	4.78	1.71	1.38
7	323.0291	3.537884	0.851401	betaine	-0.93	-4.17	-7.94	-4.70	0.53	0.95	0.98	1.78
8	606.0748	4.036123	0.851434	Octoluse Bisphosphate	1.06	-3.88	-4.69	0.24	0.15	1.00	1.04	0.28
9	565.0482	4.056136	0.857477	tryptophan	0.44	-3.75	-4.18	0.01	0.05	1.93	1.71	0.22
10	402.9949	2.973083	0.84958	thiamine-phosphate	0.12	-3.73	-2.99	0.87	0.01	1.34	1.15	3.48
11	180.0657	2.219842	0.858241	fumarate	-2.93	-3.27	-6.82	-6.49	0.88	0.51	3.44	1.03
12	203.0819	1.413762	0.840261	FMN	1.54	-2.86	-1.06	3.34	1.17	1.98	0.65	4.25
13	203.0819	1.505575	0.858171	asparagine	-1.04	-2.73	0.10	1.79	0.62	2.12	0.10	3.83
14	341.1089	2.038149	0.846411	glutathione disulfide	-1.96	-2.52	-0.13	0.43	1.29	1.15	0.39	0.24
15	421.0756	1.887725	0.851835	CMP	-1.08	-2.37	1.97	3.26	0.47	1.60	1.10	1.82
16	241.0827	2.019653	0.856852	GMP	1.22	-2.33	-2.11	1.44	1.97	4.11	2.86	3.62
17	344.0691	2.006949	0.846896	UDP	-0.13	-2.28	-1.68	0.47	0.10	4.33	3.04	0.73
18	424.039	1.499295	0.860667	aspartate	-0.40	-1.99	2.16	3.75	0.64	3.32	2.82	5.07
19	264.1045	1.446013	0.858174	trehalose/sucrose	1.55	-1.89	-1.60	1.84	3.11	3.67	2.71	3.08
20	866.1249	1.45047	0.857708	Cellobiose	1.55	-1.89	-1.60	1.84	3.11	3.67	2.71	3.08
21	117.0186	2.093047	0.854168	N-Acetyl-L-alanine	-1.80	-1.77	0.08	0.05	0.78	1.01	0.38	0.06
22	171.0065	3.843684	0.849186	IMP	-0.41	-1.66	-1.07	0.18	0.38	2.09	1.54	0.45
23	253.0099	2.067247	0.861783	Pyroglutamic acid	-1.85	-1.53	-0.12	-0.43	0.64	0.67	0.41	0.80
24	368.9989	3.985863	0.849202	S-methyl-5--thioadenosine	-0.27	-1.28	-1.28	-0.28	0.15	1.34	1.39	0.43
25	266.0707	1.685908	0.833351	ribose-phosphate	-0.60	-1.15	0.82	1.37	0.75	1.65	1.10	2.80
26	296.0806	2.066397	0.852619	N-acetyl-L-ornithine	0.30	-1.10	-1.11	0.30	0.35	2.75	2.67	0.64
27	383.	3.042	0.771	Acetyllysin	0.05	-0.96	-0.98	0.04	0.11	1.80	2.12	0.13

	1152	196	733	e								
28	229.0112	2.020989	0.85325	adenosine	0.89	-0.91	-1.32	0.48	0.93	2.14	2.15	2.26
29	375.131	2.323842	0.84781	xanthosine-5-phosphate	-0.18	-0.89	-0.73	-0.01	0.04	1.82	2.08	0.03
30	176.935	4.759889	0.852717	2-Isopropylmalic acid	0.23	-0.74	-0.66	0.30	0.24	1.32	1.66	0.68
31	128.0341	1.83335	0.853449	dCDP	-0.36	-0.47	0.46	0.58	0.07	1.29	0.49	2.60
32	168.0656	2.160493	0.853901	xanthosine	0.45	-0.45	-0.52	0.37	1.07	1.80	1.32	1.07
33	114.0551	10.95572	0.73141	p-hydroxybenzoate	-0.33	-0.42	-0.22	-0.14	0.67	0.25	1.34	0.49
34	225.0392	11.50664	0.84889	Sedoheptoluse bisphosphate	-0.26	-0.24	-0.07	-0.09	0.28	0.00	0.14	0.08
35	145.0301	1.69376	0.833608	cystathionine	0.19	-0.23	-1.06	-0.64	0.54	0.38	1.94	0.55
36	218.1029	1.981234	0.860063	hypoxanthine	-0.22	-0.19	-0.01	-0.04	0.52	0.74	0.11	0.03
37	137.0232	1.572158	0.857927	glutamine	-0.07	-0.16	-0.09	0.00	0.28	0.01	0.07	0.06
38	367.0198	1.393888	0.84899	UDP-D-glucose	-0.14	-0.14	-0.10	-0.09	0.64	0.59	0.14	0.02
39	131.0814	6.98723	0.856877	Kynurenine	0.22	-0.11	-0.34	-0.02	0.22	0.36	1.13	0.16
40	399.0131	5.573004	0.850927	riboflavin	-0.10	-0.09	-0.13	-0.14	0.07	0.04	0.50	0.29
41	319.0463	5.199954	0.849735	Thiamine pyrophosphate	-0.03	-0.09	-0.05	0.01	0.12	0.54	0.56	0.12
42	146.0447	5.07694	0.840613	Octoluse 8/1P	0.10	-0.08	-0.32	-0.14	0.20	0.50	0.53	0.25
43	742.0695	3.301201	0.735053	valine	0.22	-0.08	-0.36	-0.06	0.27	0.36	1.11	0.22
44	664.118	1.939427	0.662212	cyclic-AMP	0.27	-0.02	0.62	0.91	0.55	0.64	1.54	1.10
45	662.1027	8.18236	0.852802	tryptophan	0.28	-0.01	-0.40	-0.11	0.20	0.13	0.99	0.61
46	175.0351	1.743987	0.85161	glucose-6-phosphate	0.35	0.04	1.96	2.27	0.75	0.07	0.43	3.75
47	129.1023	6.07219	0.850308	thiamine	0.00	0.05	-0.08	-0.14	0.13	0.05	0.50	0.34
48	173.0922	2.708844	0.81459	pantothenate	0.40	0.06	-0.53	-0.18	0.33	0.03	1.38	0.97
49	130.0498	5.998872	0.854558	biotin	0.14	0.06	-0.17	-0.09	0.19	0.08	0.77	0.16
50	187.0716	1.777959	0.832413	shikimate-3-phosphate	0.04	0.06	0.20	0.18	0.44	0.47	1.26	0.37
51	188.0556	1.504867	0.772704	N-acetyl-glutamine	0.04	0.09	0.16	0.10	0.02	0.01	1.50	1.00
52	300.0466	1.719046	0.848407	guanine	-0.13	0.13	0.24	-0.02	0.45	0.03	0.79	0.22
53	179.0552	1.501844	0.85144	inosine	-0.21	0.17	1.76	1.37	0.00	0.07	2.49	1.18
54	134.0294	2.00565	0.855251	dGMP	0.40	0.25	0.12	0.27	0.68	0.33	0.71	0.24
55	148.0426	3.28745	0.850251	D-sedoheptulose-1/7-phosphate	0.19	0.26	0.12	0.05	0.03	0.17	0.99	0.45
56	133.0131	1.936306	0.677158	methionine	-0.17	0.29	0.50	0.05	0.16	1.54	0.85	0.13

57	145.0971	1.390545	0.850053	UDP-N-acetyl-glucosamine	-0.21	0.40	0.18	-0.42	0.17	0.40	0.66	0.17
58	205.0347	2.536442	0.851966	proline	-0.88	0.40	-1.20	-2.48	0.33	0.24	0.81	1.84
59	289.1155	1.833144	0.851898	a-ketoglutarate	0.38	0.42	1.06	1.02	1.23	1.41	2.15	1.78
60	207.077	2.012048	0.833829	tyrosine	0.15	0.48	0.51	0.18	0.70	2.96	2.09	1.13
61	267.0725	1.519962	0.766428	Aminoadipic acid	0.22	0.49	0.01	-0.26	0.38	1.51	0.22	1.52
62	347.0395	2.04751	0.799432	N-acetyl-glutamate	0.26	0.53	0.47	0.19	0.21	1.07	0.92	0.36
63	135.0301	3.948531	0.850648	acetyl-CoA	0.12	0.55	1.77	1.34	0.04	2.12	2.55	2.32
64	112.4286	1.409344	0.858314	arginine	0.12	0.56	0.53	0.09	0.51	1.82	2.03	0.09
65	154.0611	1.914433	0.856739	glutathione	0.05	0.57	0.97	0.45	0.03	1.40	2.23	1.89
66	282.0861	1.459852	0.857308	ornithine	-0.04	0.58	0.55	-0.07	0.34	0.41	2.33	0.09
67	150.0411	2.037107	0.853763	thymidine	0.18	0.59	0.36	-0.04	0.44	1.94	2.04	0.31
8	362.0511	1.499073	0.851382	L-arginino-succinate	-0.38	0.63	2.28	1.27	0.38	1.49	2.82	0.84
69	611.1408	2.658341	0.853422	N-acetyl-glucosamine-1/6-phosphate	0.02	0.67	0.51	-0.14	0.21	2.95	2.74	0.61
70	306.0765	1.728165	0.823201	N-carbamoyl-L-aspartate	0.61	0.73	0.23	0.11	0.87	0.40	0.17	0.02
71	145.0607	2.06878	0.715853	uridine	0.12	0.75	0.56	-0.06	0.21	2.06	1.65	0.42
72	259.022	1.509566	0.783648	pyridoxine	-0.08	0.76	0.58	-0.26	0.11	3.64	3.39	2.73
73	178.0714	1.853829	0.854485	sn-glycerol-3-phosphate	0.08	0.83	0.36	-0.39	0.00	2.49	1.50	1.29
74	177.0395	2.04771	0.750985	xanthine	-0.02	0.84	0.62	-0.24	0.23	2.54	2.09	1.04
75	313.0589	2.024257	0.820586	citrate/isocitrate	0.48	0.85	0.79	0.42	0.68	1.42	1.53	1.24
76	109.5264	1.386311	0.855701	adenosine 5--phosphosulfate	0.31	0.85	0.50	-0.04	0.53	2.48	2.30	0.33
77	338.989	1.485925	0.818313	O-acetyl-L-serine	-0.14	0.93	0.85	-0.22	0.73	3.92	3.35	1.01
78	455.1014	6.339029	0.859511	2_3-dihydroxybenzoic acid	-1.45	0.94	-0.60	-2.99	2.03	1.58	1.11	3.67
79	784.1508	1.505536	0.850999	cytidine	-0.05	0.96	0.86	-0.15	0.01	4.59	3.03	0.30
80	321.0496	1.780281	0.860946	malate	-0.10	0.99	0.15	-0.95	0.12	1.90	0.05	4.07
81	346.0558	1.441355	0.856271	lysine	1.42	1.02	-0.06	0.34	1.83	1.76	0.14	1.05
82	686.1423	1.567711	0.853065	lipoate	0.04	1.08	0.61	-0.43	0.38	3.09	2.51	2.90
83	251.0776	4.043802	0.84958	FAD	-0.14	1.11	0.56	-0.69	0.23	3.17	0.87	1.06
84	250.0937	2.100759	0.846352	NADP+	0.30	1.11	1.08	0.27	0.04	0.65	1.58	0.25
85	386.0172	1.486119	0.856649	D-gluconate	-0.02	1.15	1.23	0.05	0.30	2.63	3.13	0.20

86	289.0352	1.507047	0.851621	2-dehydro-D-gluconate	-0.21	1.28	1.75	0.27	0.04	2.48	1.42	0.27
87	258.0375	1.453563	0.828056	histidine	0.30	1.30	1.00	0.01	0.46	2.73	3.55	0.11
88	195.0502	2.024109	0.852796	dTMP	-0.94	1.31	1.59	-0.66	1.19	1.38	2.20	1.03
89	199.0007	1.550444	0.856554	homoserine	-2.41	1.32	-1.46	-5.18	0.76	0.25	0.97	1.45
90	242.078	2.027355	0.788688	glucono-Î´-lactone	0.47	1.33	1.05	0.18	0.65	2.37	1.75	0.20
91	239.0147	1.507822	0.829343	myo-inositol	-0.17	1.38	1.11	-0.44	0.91	4.50	3.63	1.23
92	221.0598	1.489268	0.854986	citrulline	-0.20	1.46	1.22	-0.43	0.35	3.66	2.77	1.07
93	328.0454	3.954113	0.838432	succinyl-CoA/methylmalonyl-CoA	-0.26	1.66	1.51	-0.42	0.34	1.03	2.36	0.81
94	689.0877	2.038819	0.852447	cyclic bis(3-->5-)dimeric GMP	-0.18	1.68	1.61	-0.24	2.83	3.02	2.29	0.14
95	766.1091	1.525817	0.835367	Phenylpropiolic acid	0.14	1.75	1.23	-0.37	0.00	0.58	1.85	0.47
96	322.0445	3.260484	0.848054	coenzyme A	-1.70	1.77	1.48	-1.99	1.48	2.14	1.76	3.87
97	174.0874	1.793035	0.851756	D-erythrose-4-phosphate	0.19	1.89	1.83	0.14	0.42	1.66	1.94	0.01
98	191.019	1.979981	0.851608	Methylcysteine	0.95	2.07	1.70	0.58	0.58	1.09	0.71	0.54
99	341.1089	1.499742	0.852927	S-ribosyl-L-homocysteine-nega	0.12	2.14	0.40	-1.63	0.11	2.81	0.72	1.16
100	243.0804	1.504422	0.852072	deoxyinosine	0.31	2.21	1.33	-0.57	0.79	2.89	2.21	0.13
101	116.0711	1.985581	0.85367	NADH	-2.59	2.54	3.62	-1.52	1.44	0.68	3.51	0.63
102	132.0291	1.759809	0.850709	trehalose-6-Phosphate	2.73	2.56	0.30	0.47	3.62	3.26	0.95	2.36
103	131.045	1.46988	0.853972	deoxyadenosine	0.33	2.69	1.93	-0.43	0.47	4.44	2.27	0.21
104	173.1035	1.516454	0.850518	D-glucosamine-6-phosphate	0.68	2.77	1.61	-0.49	0.69	1.86	0.67	0.30
105	160.0605	1.466613	0.852018	glucosamine	0.42	2.83	2.92	0.51	0.89	3.49	2.96	0.18
106	426.0121	2.080937	0.848104	NAD+	-0.69	3.58	2.11	-2.15	0.07	2.46	0.79	1.78
107	266.091	1.819532	0.852153	Pyrophosphate	0.22	4.02	3.37	-0.43	0.55	5.90	4.13	0.82
108	187.108	1.889188	0.850813	Uric acid	-0.31	4.32	3.55	-1.08	0.17	4.38	2.87	0.74
109	808.1196	2.336574	0.830013	dephospho-CoA	-1.36	11.89	2.10	-11.15	1.16	1.83	1.11	0.44
110	145.0132	2.367599	0.838086	Cystine	1.04	12.24	11.20	0.00	2.09	7.53	1.86	0.43
111	153.0182	1.50954	0.803857	S-adenosyl L-homoCysteine	-0.86	12.98	13.85	0.00	1.67	8.01	6.35	#DIV/0!
112	175.0602	1.598831	0.850469	prephenate	0.46	13.61	13.14	0.00	0.07	5.34	1.52	0.75

113	193.0346	1.51109	0.831777	guanosine	0.08	14.42	1.34	-13.00	0.45	1.36	2.89	1.14

Key: med Mz: Median *m/z* for metabolites, medRt: Median Retention Time, Max Quality: quality of peaks detected, compound: Metabolite, CSH4 - WG350: log_2 of fold change and between CSH4 and WG350, CSH4 - CSH4 (S): log_2 of fold change between CSH4 and CSH4 salt, WG350 - WG350 (S): log_2 of fold change between WG350 and WG350 salt, CSH4 (S)- WG350 (S):): log_2 of fold change between CSH4 salt and WG350 salt

Table S2: Concentration of metabolites added to LB to measure effect of metabolites on Fluorescence *in vivo* (Related to Figure 6)

S. no.	Metabolite	Concentration (mM)
1	Alanine	200
2	Betaine	200
3	Proline	200
4	Serine	200
5	TMAO	200
6	Malate	100
7	Malonate	100
8	Fumarate	100
9	Succinate	100
10	KCL	350
11	NaCl	350
12	Sucrose	400
13	Sorbitol	400